Journal of Volcanology and Geothermal Research 432 (2022) 107706

Contents lists available at ScienceDirect

Journal of Volcanology and Geothermal Research

journal homepage: www.journals.elsevier.com/journal-of-volcanology-and-geothermal-research

The recent volcanism of Flores Island (Azores): Stratigraphy and eruptive history of Funda Volcanic System

Mariana Andrade [a,b,c,*], Adriano Pimentel [d,e], Ricardo Ramalho [f,a,g], Steffen Kutterolf [h], Armand Hernández [i]

[a] Universidade de Lisboa, Faculdade de Ciências, Instituto Dom Luiz, Lisboa, Portugal
[b] Departamento de Geologia, Faculdade de Ciências da Universidade de Lisboa, Campo Grande, Lisboa, Portugal
[c] Geosciences Barcelona (Geo3BCN-CSIC), Barcelona, Spain
[d] Centro de Informação e Vigilância Sismovulcânica dos Açores (CIVISA), 9500-321 Ponta Delgada, Azores, Portugal
[e] Instituto de Investigação em Vulcanologia e Avaliação de Riscos (IVAR), Universidade dos Açores, 9500-321 Ponta Delgada, Azores, Portugal
[f] School of Earth and Environmental Sciences, Cardiff University, Park Place, Cardiff CF10 3AT, United Kingdom
[g] Lamont-Doherty Earth Observatory of Columbia University, New York, USA
[h] GEOMAR Helmholtz Centre for Ocean Research, Kiel, Germany
[i] Universidade da Coruña, GRICA Group, Centro de Investigacións Científicas Avanzadas (CICA), Rúa as Carballeiras, 15071 A Coruña, Spain

ARTICLE INFO

Keywords:
Ocean island volcanoes
Monogenetic volcanism
Strombolian eruptions
Phreatomagmatism
Glass geochemistry
Holocene volcanism

ABSTRACT

Monogenetic volcanoes occur in many different geotectonic settings and are usually small and short-lived. They can experience a variety of eruptive styles, even during the same eruption. In monogenetic volcanic fields, volcanism usually migrates to different locations over time, making volcanic hazard assessment very challenging. The eruptive history of a volcanic region, including the size, style, and location of previous eruptions, provides valuable information to help predict the behaviour of future volcanic events and their associated hazards. Here, we reconstruct for the first time the eruptive history of the Funda Volcanic System (FVS), one of the most recent (~3 ka) monogenetic eruptive centres of Flores Island (Azores), based on a detailed tephrostratigraphic work coupled with geochemical analysis of glass shards and radiocarbon dating. We identified at least three volcanic events at FVS spaced by time intervals of ~100 yr. The first event (3430 cal yr BP) was a small Strombolian eruption, the second event (3330 cal yr BP) started as a violent Strombolian eruption and may have ended as phreatomagmatic, and the third event (3250 cal yr BP) was exclusively phreatomagmatic. Our results demonstrate that volcanism at the FVS was more prolonged and recurrent than previously reported. Moreover, we show that the FVS experienced different eruptive styles in a short timeframe, ranging from small basaltic eruptions to violent explosive phreatomagmatic events. Such diversity of eruptive styles results in different volcanic products, which have different hazard implications. Our new results contribute to the knowledge of the recent volcanic activity of Flores Island, and we anticipate them to be of paramount importance for future volcanic hazard assessment studies.

1. Introduction

Monogenetic volcanoes are the most common volcanoes on earth (Wood, 1980) and may form in many volcanic environments, under very different tectonic contexts (Martí et al., 2011). They are dominantly mafic in composition (Németh, 2010) and can show a large diversity of eruptive styles. They range from effusive to violent explosive eruptions, resulting in a variety of volcanic products and morphologies, including scoria cones, maars, tuff rings, tuff cones, lava domes and even small shield volcanoes (Connor and Conway, 2000; Martí et al., 2011).

Although monogenetic eruptions usually occur over short timescales (days to years), there may be considerable changes in the eruptive style of a single eruptive event due to changes in the volume and velocity of ascending magma (Zanon et al., 2009) and/or due to magma/water interactions at near surface phreatic levels or lakes (Németh et al., 2012). Changes in eruptive styles from Strombolian to phreatomagmatic are described for many monogenetic volcanic fields such as La Garrotxa, Pinacate, Eifel, Bakoni-Balaton and Hopi Buttes (Houghton and

* Corresponding author at: Faculdade de Ciências da Universidade de Lisboa, Edifício C6, sala 6.2.79, Campo Grande 1749-016, Lisboa, Portugal.
E-mail address: mdandrade@fc.ul.pt (M. Andrade).

https://doi.org/10.1016/j.jvolgeores.2022.107706
Received 27 July 2022; Received in revised form 20 October 2022; Accepted 25 October 2022
Available online 29 October 2022

Schmincke, 1989; Houghton and Nairn, 1991; Gutmann, 2002; Kereszturi et al., 2011; Martí et al., 2011; Latutrie and Ross, 2020), including monogenetic volcanoes from different volcanic islands (e.g., Clarke et al., 2009; Pedrazzi et al., 2018; Zanon and Viveiros, 2019).

Flores is one of the least known and understood islands of the Azores Archipelago (Fig. 1a). This island did not experience any volcanic eruptions since the Portuguese settlement in the 15th century (Chester et al., 2017). Its last stage of volcanism was characterized by monogenetic effusive and explosive basaltic eruptions, that formed several scoria cones, maars, and tuff rings throughout the entire central area of the island (Morisseau and Traineau, 1985; Azevedo and Portugal Ferreira, 1999; Andrade et al., 2021). The latest volcanic events dated ~3 ka and clustered at two volcanic centres, denominated as the Funda Volcanic System (FVS) and the Comprida Volcanic System (CVS) (Fig. 1b; Andrade et al., 2021). Critically, proximal sequences suggest that in both cases, eruptions started as Strombolian and ended with violent phreatomagmatic activity (Morisseau and Traineau, 1985; Azevedo and Portugal Ferreira, 1999; Andrade et al., 2021). This highlights the role of magma/water interactions in modulating eruptive behaviour in this area.

Given the relatively young age and high explosiveness of Flores last volcanic events, the study of potential volcanic hazard at Flores Island is of paramount importance for the safeguarding of the local populations. Moreover, to robustly predict the behaviour of future volcanic events and their associated hazards, a detailed reconstruction of the latest events, their eruptive behaviour and source parameters is critical. Accordingly, in this paper, we report for the first time on a detailed tephrostratigraphy coupled with geochemical analysis of glass shards

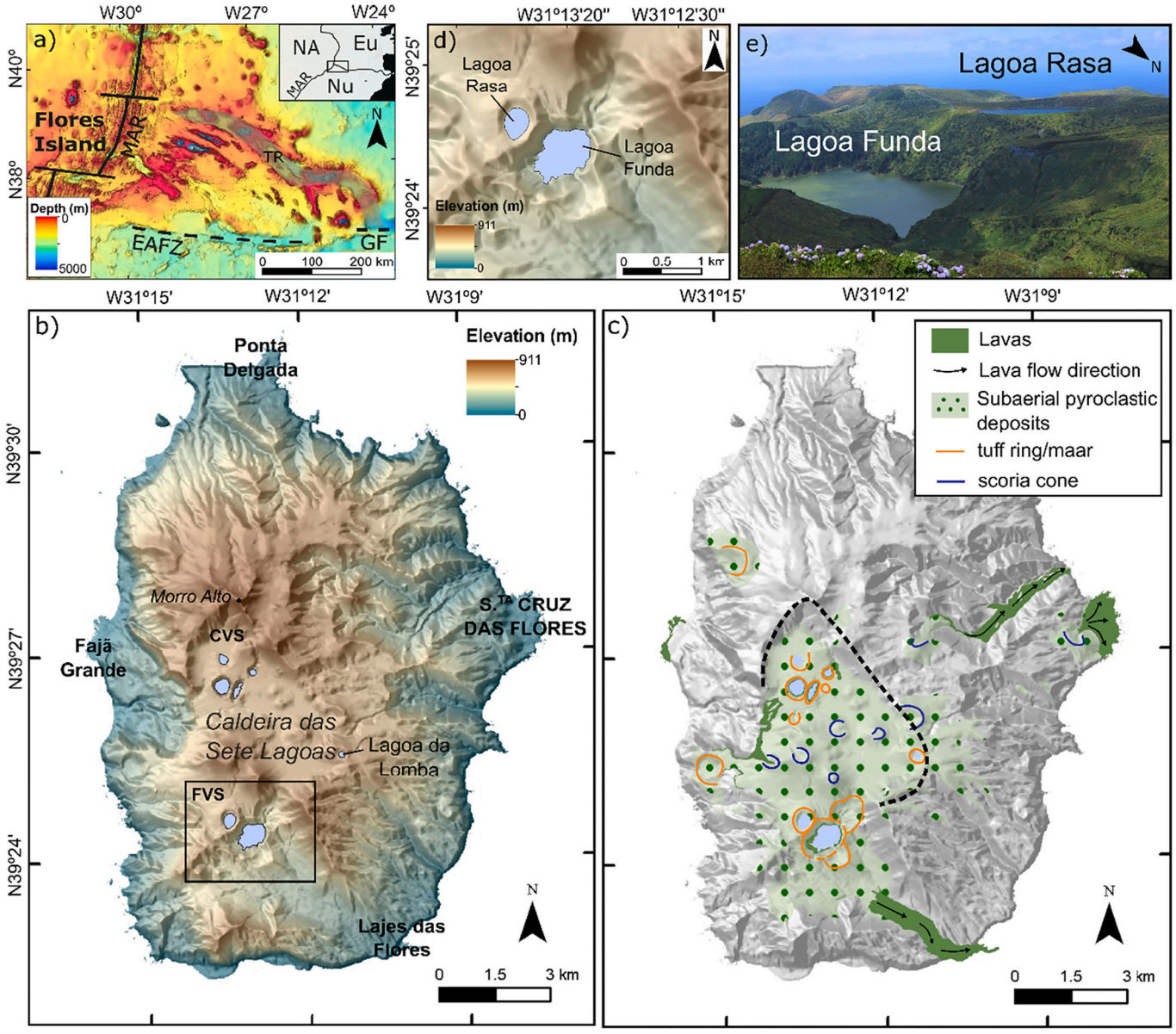

Fig. 1. Flores Island location and main characteristics of the study site. a) Bathymetric map of the North Atlantic at the Azores triple junction showing the location of Flores. MAR – Mid-Atlantic Ridge, EAFZ – East Azores Fracture Zone, GF – Gloria Fault. Bathymetry from EMODnet Bathymetry Consortium (2018); Upper right inset depicts the regional setting of the Azores Archipelago within the triple junction of the North American (NA), Eurasian (Eu) and Nubian (Nu) lithospheric plates; b) Digital elevation model (hillshade, UTM projection, zone 25 N) of Flores Island showing the location of the two main Holocene eruptive centres: Comprida Volcanic System (CVS) and Funda Volcanic System (FVS). The island's capital (S^{ta} Cruz das Flores) as well as the other main villages are indicated; c) Distribution of the craters and volcanic products resulting from the last stage of volcanism at Flores Island (this study). Dashed line is limiting Caldeira das Sete Lagoas; d) Detailed view of digital elevation model around Funda Volcanic System (FVS); e) Landscape photograph of Funda (maar) and Rasa (tuff ring) lakes.

and radiocarbon dating to reconstruct the eruptive history of the FVS, as well as the size and style of its eruptions. FVS hosts one of the largest and deepest maars of the Azores and exhibits a rich and complex tephrostratigraphic record; its study is therefore crucial to our comprehension of Flores' recent volcanic activity.

2. Geological setting

Flores is the westernmost island of the Azores Archipelago located in the Atlantic Ocean between latitudes N36.9°-39.7° and longitudes W24.9°-31.3° (Fig. 1a). The archipelago results from geodynamic processes related to the interaction between the triple junction of the North American, Eurasian, and Nubian lithospheric plates and a deep melting anomaly (e.g., Gente et al., 2003; Trippanera et al., 2014; Genske et al., 2016). Flores and Corvo islands lie on the North American plate (Fig. 1a), along an NNE-SSW-trending volcanic ridge subparallel to the Mid-Atlantic Ridge, in a more stable setting than the eastern islands of the archipelago.

Flores is a small oceanic volcanic island (142 km^2) with a complex geological history characterized by the activity of overlapping polygenetic volcanoes, periods of vertical crustal movements and mass wasting events (Azevedo and Portugal Ferreira, 1999, 2006; Hildenbrand et al., 2018). K/Ar geochronological data of subaerial formations indicate a maximum age of 2.16 Ma for the emersion of Flores volcanic edifice (Azevedo and Portugal Ferreira, 1999). The morphology of the island is characterized by a central upland area (above 500 m altitude) that reaches a maximum elevation of 911 m at Morro Alto (Fig. 1b). This central plateau, locally known as Caldeira das Sete Lagoas, is punctuated by scoria cones, maars, and tuff rings, and surrounded by notched valleys and cliffs with slopes higher than 40–45° (Fig. 1b and c).

The volcanostratigraphy of Flores has been divided into two main groups (Azevedo et al., 1991; Azevedo and Portugal Ferreira, 1999, 2006):

1) The Base Complex includes all deposits related to the submarine and emergent proto-insular volcanism of Plio-Pleistocene age (2.16–0.75 Ma). This unit reportedly crops out along the lower levels of coastal cliffs and is mainly composed of intensively palagonitized volcaniclastic deposits (hyalo- and hydroclastites) of breccias and tuffs, with a few basaltic and hawaiitic lavas on top.
2) The Upper Complex includes all the deposits resulting from subaerial volcanism and has been subdivided into three units: i) the Lower Unit (660–550 ka) comprising the products of the most voluminous volcanism of the island, that produced extensive and sometimes very thick lavas, with alternating subordinate pyroclastic deposits, ranging from basaltic to trachytic compositions; ii) the Middle Unit (400–230 ka) composed of the products of small feeder centres, with predominant basaltic and hawaiitic lavas and associated pyroclastic deposits; iii) the Upper Unit (?-3 ka), which includes the deposits of a period of volcanism that produced predominantly basaltic/hawaiitic pyroclastic deposits (scoria and phreatomagmatic deposits).

2.1. Flores last stage of volcanism

The last volcanic events of Flores Island occurred after a period of volcanic quiescence, which is marked by a noticeable unconformity, and were characterized by monogenetic basaltic eruptions, ranging from effusive to highly explosive (phreatomagmatic) activity (Azevedo and Portugal Ferreira, 2006). These eruptions were responsible for the formation of many of the scoria cones, maars and tuff rings found on the island (Fig. 1c). Currently, most of the recent maars and tuff rings are occupied by lakes.

Holocene volcanic activity started at least 6280 cal yrs. BP (Andrade et al., 2021) and was initially characterized by Strombolian eruptions that formed small to medium size scoria cones, most of them rooted in older craters and vents (Azevedo and Portugal Ferreira, 2006). The subsequent phreatomagmatic activity was centred at two clusters of volcanism, with eruptions firstly occurring at Funda Volcanic System (FVS; ~3360 cal yr BP) in the southern part of Caldeira das Sete Lagoas, and then at Comprida Volcanic System (CVS; ~3050 cal yr BP) in the northern sector (Morisseau and Traineau, 1985; Fig. 1b).

The maars preserve deep lakes (up to 114 m), steep slopes and diameters ranging from 280 m to ~1 km, while tuff rings have low crater rims, shallow lake depths (up to 16 m), smooth slopes, and diameters in the order of 300–400 m (Andrade et al., 2019; Fig. 1b-e). The phreatomagmatic deposits associated with the FVS and CVS are thin-bedded sequences of fine ash layers intercalated with coarser lithic-rich layers (lithics up to block size), showing lateral continuity for several hundreds of meters (Andrade et al., 2021). Proximal sequences from both volcanic centres show that different eruptive styles have occurred, with evidence of transition from magmatic to phreatomagmatic activity (Azevedo and Portugal Ferreira, 2006; Andrade et al., 2021).

3. Methods

3.1. Fieldwork

FVS pyroclastic sequence was studied in detail during two field campaigns in the summer of 2019 and 2020 to reconstruct the sequence of volcanic events and characterize the associated eruptive styles. A total of 161 stratigraphic sections were reconstructed throughout Caldeira das Sete Lagoas and the eastern side of the island. FVS deposits were systematically described in terms of thickness, grain size, components, textures, internal structures, and spatial distribution. Stratigraphic discontinuities such as paleosols and erosion surfaces were used to recognize the limits of the deposits. The maximum clast size of the deposits was obtained by averaging the length of the major axis of the five largest lithic and juvenile fragments. Representative samples were collected throughout the stratigraphic sections, including tephras, paleosols, and carbonized wood fragments. Field locations are listed in Supplementary material 1.

3.2. Eruption source parameters

Eruption source parameters were obtained from the analysis of the mapped volcanic products. The volume of tephra fall deposits was calculated applying the method of Pyle (1989) modified by Fierstein and Nathenson (1992) to the isopach maps. Tephra bulk densities were measured in the laboratories of Faculdade de Ciências da Universidade de Lisboa (Portugal) by weighing three samples of each deposit in a known volume and averaging the measurements. Erupted mass was determined based on measured tephra densities of 755–776 kg/m^3 and magnitude was calculated following Pyle (2000). Tephra volume was converted to dense rock equivalent (DRE) volume considering the tephra bulk density and a trachybasalt magma density of 2800 kg/m^3 (Pimentel et al., 2016).

Eruption column height was estimated with the method of Carey and Sparks (1986), using the 3.2 cm isopleth of lithic clasts. Mass eruption rate was determined applying the method of Wilson and Walker (1987) modified for basaltic magma compositions (Costantini et al., 2009) and intensity was calculated following Pyle (2000).

3.3. Glass geochemistry

Forty-three tephra samples were collected for glass geochemical analysis. Each sample was cleaned, manually crushed, and sieved. The 63–125 μm (4–3 Φ) fraction was mounted into acrylic tablets, filled with epoxy resin, polished, and carbon-coated for electron microprobe (EMP) analysis. Glass shards were analysed for major and minor elements using a JEOL JXA 8200 wavelength dispersive EMP at GEOMAR Helmholtz Centre for Ocean Research, Kiel (Germany) following the methods of

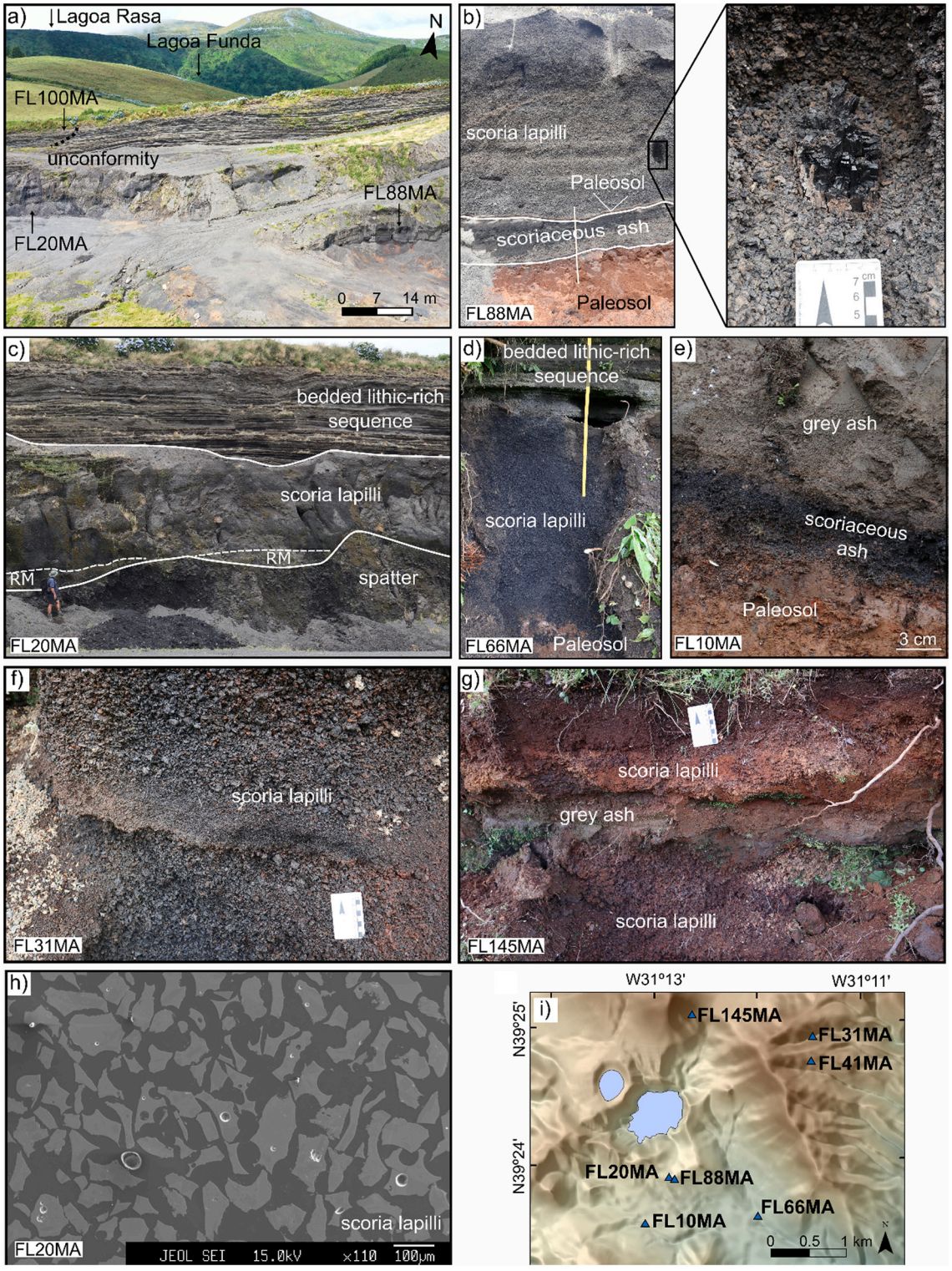

Fig. 2. Field photographs showing the relationship and the main features of the scoria deposits: a) photograph of a quarry on the rim of the SE crater, showing the location of the outcrops were proximal sequences are well exposed; b) proximal volcanic sequence, located at field site FL88MA, showing the basal ash unit of the FVS which is top limited by a thin paleosol, in turn overlapped by a thick scoria lapilli unit; magnified view shows a carbonized tree trunk still in its vertical position within the scoria lapilli. Scale (vertical white line) is 1 m; c) proximal volcanic sequence at field site FL20MA consisting of (from the base to the top): spatter accumulation, remobilized material (RM), scoria lapilli and bedded lithic-rich sequence (phreatomagmatic); d) homogeneous scoria lapilli deposit cropping out at Vale das Lajes, field site FL66MA. The lapilli deposit is overlapped by a bedded lithic-rich sequence (phreatomagmatic); scale (yellow vertical line) is 75 cm; e) scoriaceous ash unit cropping out south of FVS, field site FL10MA, which is overlapped by a greyish ash layer; f) lapilli tephra deposit located NE of FVS, field site FL31MA, showing the granulometric succession from medium to fine and back to medium grain size lapilli; g) volcanic sequence cropping out NE of FVS, showing an altered scoria lapilli layer overlaying the scoria unit with grain size variation. The two scoria units are separated by a grey ash bed; h) BSE image of scoria lapilli unit from outcrop FL20MA showing juvenile clasts with typical angular, lunate, bubble-walled and high-vesicular shapes; i) digital elevation model (hillshade) showing the location of the referred sequences. (For interpretation of the references to colour in this figure legend, the reader is referred to the web version of this article.)

Table 1
AMS radiocarbon and respective calibrated ages obtained at different FVS sequences.

Sample ID	Type of sample	Location	Lab ID	$\delta^{13}C$ (‰)	^{14}C	±	$\delta^{14}C$ (‰)	±	^{14}C age (BP)	±	Median Probability (cal yr BP)	2σ (cal yr BP)
FL01MA-5	paleosol	N39°24′11.02" W31°12′25.88"	ULA-9373	−26.1	0.674	0.0011	−326.2	1.1	3170	15	3394	−31/+19
FL41MA-1	paleosol	N39°24′43.13" W31°11′37.43"	ULA-9353	−26.0	0.646	0.0011	−354.1	1.1	3510	15	3772	−57/+33
FL80MA-1	paleosol	N39°24′54.29" W31°13′29.21"	ULA-9370	−25.6	0.652	0.0012	−347.7	1.2	3430	15	3670	−39/+52
FL88MA-3d	carbonized wood	N 39°23′53.12" W31°12′54.25"	ULA-9352	−23.2	0.680	0.0011	−320.5	1.1	3105	15	3333	−10/+42
FL88MA-3e	carbonized wood	N 39°23′53.12" W31°12′54.25"	ULA-9356	−23.3	0.669	0.0011	−331.0	1.1	3230	15	3428	+38
FL92MA	carbonized wood	N 39°23′29.94" W31°12′40.93"	ULA-9355	−23.7	0.685	0.0011	−315.5	1.2	3045	15	3254	−47/+16

Kutterolf et al. (2011).

EMP analysis included a calibrated measuring program based on international standards with a 10 μm electron beam to minimize Na loss. The ZAF correction method was used to determine oxide concentrations. Lipari obsidian (Lipari rhyolite; Hunt and Hill, 2001) and Smithsonian basaltic standard VGA99 (Makaopuhi lava lake, Hawaii; Jarosewich et al., 1980) were used to monitor accuracy, by having two measurements on each standard after every 60 single glass shard measurements. Standard deviations are <0.5% for major and < 10% for minor elements (except for MnO_2 in samples >55 wt% SiO_2).

Analyses with totals <97 wt% and > 103 wt% were removed. The rest of the analysis were normalized to 100 wt% to eliminate effects of variable post-depositional hydration and small deviations in the focus of the electron beam. The acceptable analyses of each sample (433 in total) were statistically processed to characterize the elemental compositions of each tephra. The resulting major and minor element data and their respective errors are listed in Supplementary material 2 and 3.

3.4. Radiocarbon dating

Three paleosols underlying pyroclastic units and three carbonized wood fragments directly incorporated in key pyroclastic deposits were collected for radiocarbon age determinations. To minimize sample contamination, any visible modern roots were removed. The samples were analysed at Radiochronology Laboratory of the Centre d'Études Nordiques, University of Laval (Canada) for accelerated mass spectrometer (AMS) radiocarbon dating. Before AMS ^{14}C measurements, samples underwent a HCl - NaOH - HCl treatment to remove inorganic carbons. The reported radiocarbon ages expressed as years BP were calibrated to cal yr BP with the CALIB 8.2 software, using the IntCal20 calibration curve (Stuiver et al., 2021).

4. Results and interpretations

4.1. Description and chronology of FVS pyroclastic sequence

Of the 161 stratigraphic sections reconstructed during field campaigns, the 18 most representative were selected to show the variety of deposits of FVS, their stratigraphic relationship and radiocarbon ages.

4.1.1. Scoria fall deposits

Description: In proximal areas, the pyroclastic sequence is best exposed in a quarry located on the rim of the SE crater of the FVS (Fig. 2a). At outcrop FL88MA, the basal unit of the pyroclastic sequence is conformably overlying a thick (>2 m) paleosol, and it consists of a 48 cm thick bed of dark grey scoriaceous ash. The ash unit incorporates a lens of scoria lapilli, which varies in thickness from 5 to 25 cm (Fig. 2b and Supplementary Fig. 1a). This unit contains plagioclase crystals, syenite xenoliths, rare lithic clasts, and abundant carbonized wood fragments, dated at 3430 cal yr BP (Supplementary Fig. 1a; Table 1). Its top is eroded and limited by a thin (up to 5 cm thick) paleosol.

Overlying the basal ash unit is a thick (~3.5 m) bed of black/dark grey, coarse scoria lapilli, with well-preserved scoriaceous textures, and numerous bombs. Olivine, pyroxene, and plagioclase crystals are present, as well as syenite xenoliths and carbonized wood fragments, including a tree trunk still in its original upright position, dated at 3330 cal yr BP (Fig. 2b; Table 1). It should be noted that only the portion of the trunk that was above the thin paleosol was charred, while the lower part embedded in the basal ash unit was mummified.

The thick scoria lapilli unit is laterally continuous along the quarry exposure, but the basal ash unit below is not. At field site FL20MA, approximately 70 m west of FL88MA (Fig. 2a and i), the thick scoria lapilli unit is exposed, but the basal ash is replaced by a spatter accumulation (>1.70 m thick), containing large bombs (up to 30 cm) with well-preserved fluidal shapes and large plagioclase crystals (Fig. 2c). Near the top, the spatter grades upward to scoria lapilli, which in turn is overlaid by a bed of reworked material (up to 80 cm thick), very heterogeneous in grain size, clast morphology and lithology (Supplementary Fig. 1b).

In more distal areas (>1.5 km from the centre of FVS), scoria deposits are mainly represented by a single bed of medium to coarse lapilli. Paleosols underlying this scoria unit were dated at 3390 cal yr BP and 3670 cal yr BP in two field sites, east (FL01MA) and north (FL80MA) of FVS, respectively (Table 1, see Fig. 3k for outcrop location). The scoria unit is usually homogeneous in terms of colour (black/dark grey where well-preserved), grain size and components, and the juveniles show pristine morphologies (e.g., field site FL66MA; Fig. 2d). However, there are exceptions:

1) South of FVS, the scoria lapilli unit is absent, but a thin (5 cm thick) dark grey scoriaceous ash bed is exposed between a paleosol developed on a very altered unit of lavas and a bedded lithic-rich ash sequence (e.g., field site FL10MA; Fig. 2e).
2) Northeast of FVS, the scoria lapilli unit shows internal grain size variation, grading from medium to fine lapilli and back to medium lapilli towards the top. In most places a thin oxidation crust is observed just below the fine lapilli layer (e.g., field site FL31MA; Fig. 2f). Above the fine lapilli there is an increase in the amount of lithics. The unit overlies an organic-rich paleosol, dated at 3770 cal yr BP (field site FL41MA; Fig. 2i; Table 1)

Despite the presence of some crystals and lithic clasts, scoria lapilli units are mainly composed of juveniles, which show the typical angular, lunate, bubble-walled and highly vesicular shapes (Fig. 2h).

Throughout most of FVS outcrops, another tephra layer crops out above the main scoria lapilli unit, always separated either by a grey ash unit in the more distal areas or by a bedded lithic-rich ash unit in the more proximal ones (e.g., field site FL145MA; Fig. 2g). This tephra layer consists of scoriaceous fine lapilli with abundant lithics, plagioclase and olivine crystals. South of FVS, its thickness is minimum (~5 cm) and

increases towards the north, in the direction of CVS. In most outcrops close to FVS, this unit is poorly preserved, showing a high degree of alteration evidenced by orange colours and weathering of the juvenile clasts (Fig. 2g).

Interpretation: Based on the characteristics of the deposits, such as consistent thinning and fining with distance from the source, the pristine nature of the juvenile clasts with well-preserved scoriaceous textures and the generally good sorting, these are interpreted as different facies of scoria fall deposits. The presence of spatter and large bombs reveals that transport by ballistic trajectory also played an important role in proximal areas.

4.1.2. Bedded lithic-rich ash fall and fully dilute pyroclastic density current (PDC) deposits

Description: A thin-bedded lithic-rich ash sequence overlies the main scoria lapilli unit described above (e.g., field sites FL20MA, FL01MA; Fig. 2c, Fig. 3a). In some places the contact between the two deposits is marked by an erosive surface but paleosols are absent (Fig. 3a-c).

In proximal areas, the bedded lithic-rich ash sequence is very thick (up to 15 m) and consists of beds of very fine ash intercalated with lapilli beds or ash beds with lapilli and blocks (Fig. 3d). The sequence contains large amounts of lithic fragments (Fig. 3e and j, with heterogenous lithologies (basaltic lavas and hydrothermally altered clasts and subordinate syenite and gabbroic xenoliths) and variable size from fine lapilli to blocks. Juveniles are rare but when present, they are usually dense, sub-rounded and blocky (Fig. 3e and j). Loose olivine and plagioclase crystals are also frequently present in this unit. Many of the ash beds contain bomb-sag structures, wavy- and cross-stratifications (Fig. 3d), and accretionary lapilli (with diameters up to 0.5 cm) (Fig. 3f). Most beds are internally massive, but some show normal or inverse grading. This unit mantles the landscape all over the FSV area, but locally tends to be topographically controlled, thickening in depressions (Fig. 3g). In different places south of FVS an unconformity is present within this sequence (e.g., field sites FL100MA and FL81MA; Fig. 3h and i). However, there is no apparent change either in the type or lithologies of the deposits above and below the unconformity. In more distal areas and west of FVS, this lithic-rich ash sequence is characterized by a greyish very fine ash unit locally intercalated with coarser ash beds (Fig. 3b).

Interpretation: Based on the characteristics of the deposits, such as thin-bedding, lithic-rich nature, abundance of very fine ash, presence of accretionary lapilli, and wavy- and cross-stratifications, these are interpreted as resulting from simultaneous deposition of ash fallout and fully dilute PDCs (surges) associated with phreatomagmatic activity. The presence of bomb-sag structures give evidence for ballistic ejecta in proximal areas.

4.1.3. Dense PDC deposit

Description: In proximal areas southeast of FVS a massive deposit crops out in some places over the bedded lithic-rich ash sequence. This massive deposit is composed of lithic clasts supported in a grey ash matrix (Fig. 4) and is strongly controlled by the local topography, filling the valleys of Ribeira das Lajes and Ribeira Seca, where its reaches up to 3.5 m and 4 m in thickness, respectively. This matrix-supported deposit is heterogeneous in both grain size and lithology (Fig. 4a-b). It contains a large amount of lithics, including basaltic lavas, hydrothermally altered clasts, altered pumice clasts, few syenite xenoliths and rare plagioclase and olivine crystals. Lapilli-size lithics are dominant, although large blocks (up to 15 cm) are common in certain locations. Several fragments of carbonized wood were found near the base of this unit at field site FL92MA (Fig. 4b), one of them dated at 3250 cal yr BP (Table 1). Downslope, the deposit sometimes exhibits lateral and vertical internal grain size variations, with the larger lithic blocks deposited in the centre of the valleys and/or on the top of the sequence.

Interpretation: Based on the characteristics of the deposit, such as the topographically controlled distribution, matrix-supported nature, poor sorting, abundance of lithic clasts, variation of internal structures, and the presence of carbonized wood fragments, it is interpreted as resulting from deposition of high particle concentration granular fluid-based currents (dense PDCs) associated with phreatomagmatic activity. However, the occurrence of charcoal reveals the currents were hot enough to incinerate vegetation.

4.2. Geochemistry of FVS deposits

Glass shard compositions of the FVS deposits are relatively homogeneous, with 46–50 wt% of SiO_2 and 5–9 wt% of total alkalis ($Na_2O + K_2O$), plotting in the trachybasalt field, excluding a number of analyses that plot as tephrite/basanite and phonotephrite (Fig. 5a). The variation diagrams of selected major elements vs CaO show a general trend that is consistent with the stratigraphic position of the samples. Overall, geochemical compositions become less evolved towards the top of the pyroclastic sequence. Four different geochemical populations were distinguished based on geochemical similarities but also based on the stratigraphic position (Fig. 5a-e).

Samples from the basal unit of the FVS (scoriaceous ash from field sites FL88MA and FL10MA) and the spatter accumulation (field site FL20MA; Fig. 2) show a large geochemical variability, with CaO contents ranging from 6 to 10 wt% (yellow symbols in Fig. 5b-e). Samples from the thick scoria lapilli unit collected at proximal and distal sites (e.g., field sites FL88MA, FL20MA, FL66MA, FL145MA; Fig. 2) are characterized by CaO contents between 8.5 and 10.5 wt% (red symbols Fig. 5b-e). In locations where the scoria lapilli unit is characterized by an internal grain size variation (e.g., field site FL31MA, Fig. 2f), only the samples below the fine lapilli fit this geochemical group. The scoria lapilli above the grain size variation (blue symbols), are slightly less evolved, as shown by the increase in MgO and decrease of SiO_2 contents (Fig. 5b-c), and their CaO contents between 9 and 11 wt% (Fig. 5b-e).

The scoria samples collected from the bedded lithic-rich ash sequence (Fig. 3) are very heterogeneous, with glass analyses lying in the trachybasalt field but also in the trachyte and basaltic trachyandesite fields (beige symbols in Fig. 5a). This suggests that at least some of the clasts are not juveniles but could be lithics instead.

5. Discussion

5.1. Reconstruction of FVS eruptive history

We reconstruct the eruptive history of the FVS by combining tephrostratigraphy with geochronology and glass geochemistry, with particular focus on the timing of events and their eruptive styles. The base of the FVS pyroclastic sequence was recognized by the presence of a well-developed paleosol, which indicates a relatively long period of volcanic quiescence, in the order of 1300 yr (Andrade et al., 2021). Based on the presence of stratigraphic discontinuities, such as paleosols and erosion surfaces, we distinguished at least three volcanic events, which were named FVS1, FVS2 and FVS3 (Fig. 6):

FVS1 is the oldest eruption recorded in the FVS pyroclastic sequence, which occurred at approximately 3430 cal yr BP. It was a Strombolian eruption that built a small scoria cone (or cones), nowadays partially buried below the rim of the SE crater of the FVS (spatter accumulation at field site FL20MA, Fig. 2b and Fig. 6). This eruption likely also emitted the lavas of Lajes das Flores, on the southeast end of the island (Fig. 1b and c; Morisseau and Traineau, 1985). The position of the outcropping portion of the scoria cone suggests that the source area of FVS1 eruption was located roughly at the same site where the SE crater of the FVS is located now. Erosion of small scoria cones can be a rapid process in humid environments like Flores (Vespermann and Schmincke, 2000), but in this case, the cone was most likely destroyed by the later explosive activity related to the formation of the present-day crater. The products of FVS1 eruption are found on a small area, with ash dispersion limited to proximal areas south and southeast of FVS (e.g., field sites FL10MA and FL88MA). When compared with other tephras of the FVS, glass

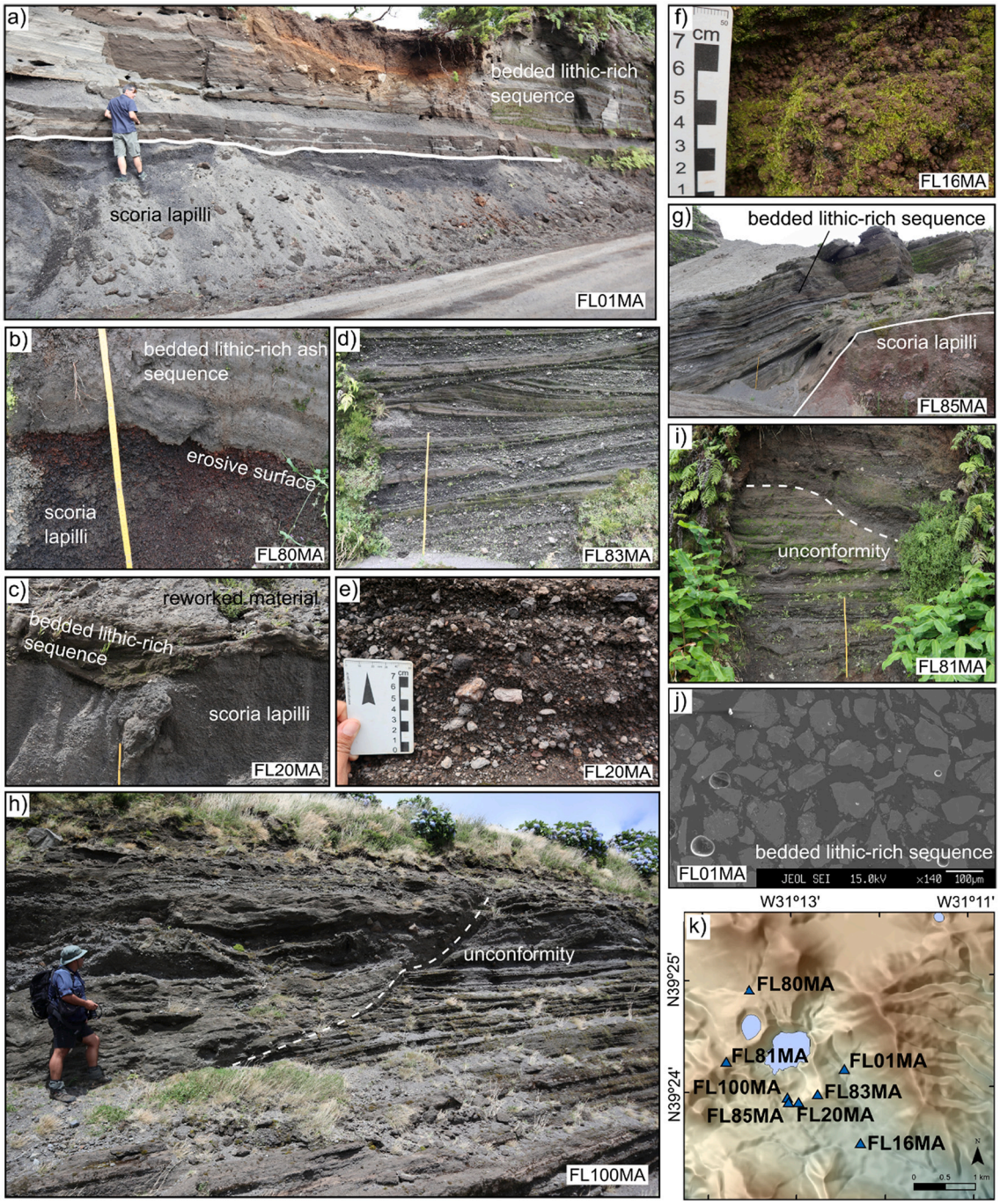

Fig. 3. Field photographs showing the main features of the bedded lithic-rich sequence (phreatomagmatic); a) volcanic sequence in a proximal site of FVS, FL01MA, showing the bedded sequence overlaying a homogeneous lapilli unit of scoriae. There is an erosive contact between the two units; b) erosive contact between the scoria unit and the bedded lithic-rich sequence at field site FL80MA and c) FL20MA; d) very proximal sequence on the rim of the SE crater of FVS, field site FL83MA. It shows wavy- and cross-stratification. Scale (yellow vertical line) is 1 m; e) detail of the lithic-rich lapilli fall deposits showing the grain size and compositional heterogeneity of the deposit, field site FL20MA; f) accretionary lapilli that characterizes the ash layers at field site FL16MA; g) bedded lithic-rich ash sequence covering a scoria unit. It shows that its emplacement was strongly controlled by topography. The sequence crops out in a very proximal area of FVS, field site FL85MA; h) unconformity cutting through the bedded lithic-rich sequence of FVS at field site FL100MA and i) FL81MA; j) BSE image of the bedded lithic-rich sequence at outcrop FL01MA showing the scarcity of juveniles and predominance of lithics and crystals; k) digital elevation model (hillshade) showing the location of the referred sequences. (For interpretation of the references to colour in this figure legend, the reader is referred to the web version of this article.)

shard compositions of FVS1 are slightly more evolved (higher SiO_2 content on average, higher total alkalis and lower MgO). Despite partially overlapping geochemical group 1 of Andrade et al. (2021), glass shards from FVS1 have lower CaO contents (Fig. 5). Taking into account the different glass compositions and the reduced spatial distribution of the deposits, we consider that tephras from FVS1 were not deposited at Lagoa da Lomba (see Andrade et al., 2021 for details), being therefore described here for the first time.

FVS2 eruption occurred ~100 years after FVS1, as the presence of a thin paleosol (Fig. 2b) and the age obtained from a carbonized tree trunk (3330 cal yr BP; Fig. 6) so suggest. The tree was rooted in the older well-developed paleosol (at the base of the FVS pyroclastic sequence) and the

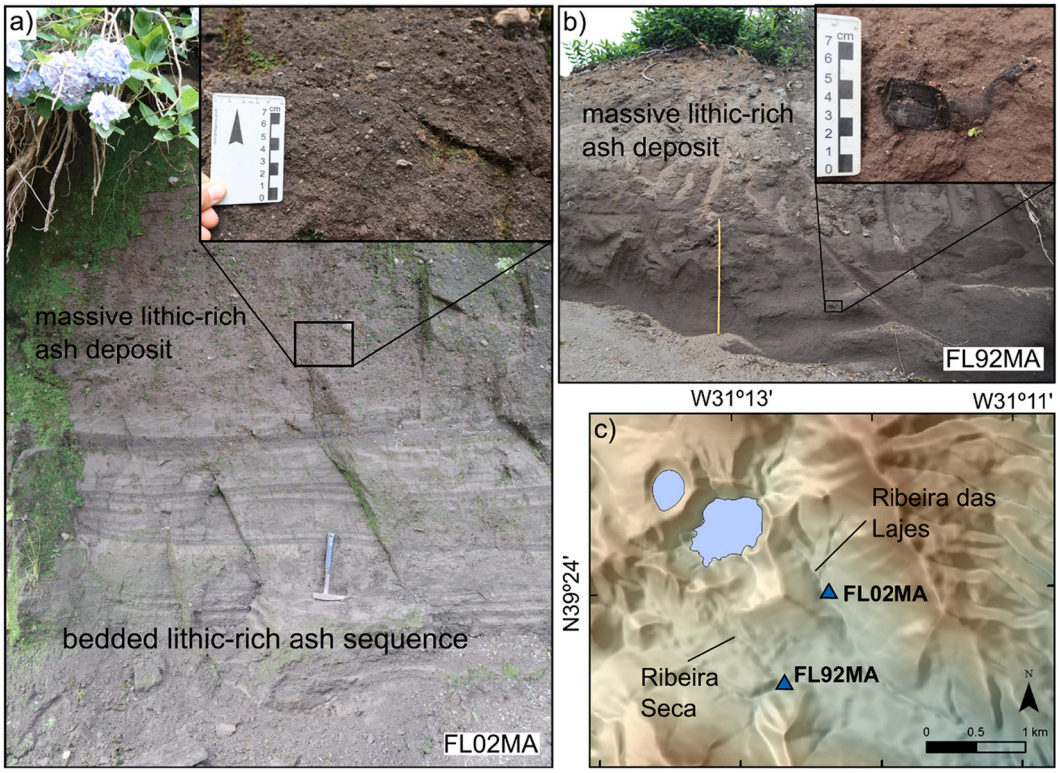

Fig. 4. Field photographs of the massive lithic-rich ash deposit; a) massive lithic-rich ash deposit overlaying the bedded lithic-rich sequence at field site FL02MA, located at Ribeira das Lajes valley; inset shows the grain size and lithological heterogeneity of the massive deposit; b) massive lithic-rich ash deposit from field site FL92MA, located at Ribeira Seca valley. Scale (yellow vertical line) is 1 m. Inset shows one of the charcoal fragments found at the bottom of the deposit; c) digital elevation model (hillshade) showing the location of the referred sequences. (For interpretation of the references to colour in this figure legend, the reader is referred to the web version of this article.)

deposition of the FVS1 ash was not hot enough to carbonize it. Yet, the subsequent deposition of the FVS2 scoria lapilli at higher temperature carbonized the portion of the tree that remained above the thin paleosol. This eruption has been previously identified and described by Andrade et al. (2021), and an age of approximately 3660 cal yr BP was estimated based on the age-depth model constructed for Lagoa da Lomba. However, the new age presented here (Table 1) indicates that FVS2 eruption occurred ~300 yr later than previously proposed. Although Morisseau and Traineau (1985) present a single age that is compatible with all the three events of the FVS, its most probable age is similar to the age we now propose for FVS2 eruption (Fig. 6c).

FVS2 eruption also formed a scoria cone (or cones) that partially overlaps the previous edifice(s) (FVS1). This second Strombolian eruption was larger than the FVS1 event, as the associated scoriae are widely dispersed along the central part of the island. It is important to highlight the internal grain size variation that characterizes the FVS2 deposit in some areas, and the upwards increasing lithic content of the deposit. As discussed in Andrade et al. (2021), the observed grain size variation can be interpreted as resulting from changes in wind speed and/or direction, or from a brief fluctuation of the eruption rate, which is translated as an oscillation of the eruption column height (column unsteadiness) (Carey and Sparks, 1986). The increase in lithic content can be associated with the enlargement of the crater, erosion and widening of the conduit (Sulpizio et al., 2005) and/or with the initiation of a phreatomagmatic pulse (Barberi et al., 1989; Martí et al., 2011; Pimentel et al., 2015).

Glass shard compositions of the FVS2 deposit are consistent with geochemical groups 1 and 2 of Andrade et al. (2021) (Fig. 5). This supports the correlation between subaerial and lacustrine tephras previously proposed by Andrade et al. (2021), confirming the good preservation of the FVS2 Strombolian eruption deposits in the sedimentary record of Lagoa da Lomba. The slightly larger compositional range observed for the subaerial samples (especially for the scoria lapilli below the grain size change; plotted in red Fig. 5b-e) may be due to the higher number of samples now analysed, which may reflect a higher spatial and temporal geochemical variability within the tephras of this event, when compared with the few lacustrine samples analysed by Andrade et al. (2021).

FVS2 exhibits a compositional trend (Fig. 5f), with the material erupted first being more evolved than the material erupted at the final phase of the eruption. Such compositional variations within a single eruption are frequently observed in basaltic (sensu *latu*) systems (Smith et al., 2008; Smith and Németh, 2017) and in other oceanic islands, like the 1580 and 1808 eruptions at São Jorge (Azores; Zanon and Viveiros, 2019), and the 1949 and 1971 eruptions at La Palma (Canary Islands; Klügel et al., 2000; Barker et al., 2015).

After the FVS2 Strombolian eruption, there was an important change in eruptive style, with purely magmatic activity being replaced by phreatomagmatic activity. Radiocarbon data indicate a time interval of ~80 years between the beginning of FVS2 and the emplacement of the dense PDCs found at the top of the phreatomagmatic succession. However, the absence of robust horizons (e.g., paleosols) to date the onset of the phreatomagmatic activity, and the difficulty to correlate individual subunits – and hence separate distinct volcanic episodes – within the phreatomagmatic succession, makes the reconstruction of the sequence of events after the FVS2 Strombolian phase more challenging.

The FVS pyroclastic sequence seems to be continuous in distal outcrops, suggesting a transition from Strombolian to phreatomagmatic activity during the FVS2 eruption. This is supported by the gradual increase in the lithic content towards the top of FVS2 scoria deposit. However, in proximal areas (e.g., field site FL01MA, FL80MA, Fig. 3a and b respectively), the top of the FVS2 thick scoria deposit is limited by an erosive surface, which suggests that the scoria deposit of FVS2 and

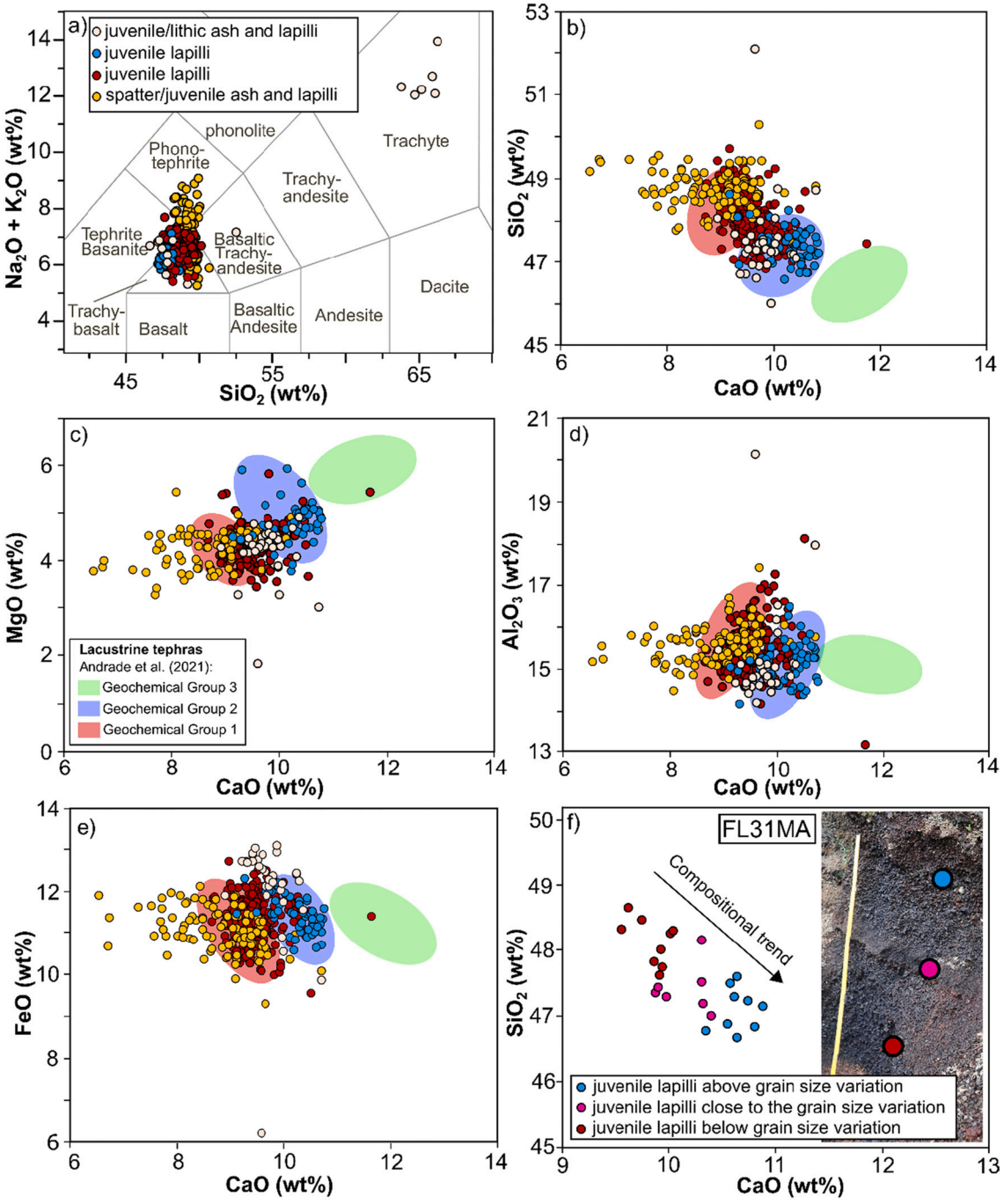

Fig. 5. a) Total alkalis vs silica (TAS) diagram, based on Le Bas et al. (1986), for the classification of glasses of FVS deposits. Compositions cluster essentially around the trachybasalt field; b-e) Variation diagrams of major elements (wt%) vs CaO (wt%) for the glasses of FVS deposits. Shaded colour areas represent the geochemical groups defined by Andrade et al. (2021) for lacustrine tephra layers reported at Lagoa da Lomba. Glasses are normalized to 100% volatile free; f) geochemical variation of the scoria deposit with the internal grain size variation from more evolved to less evolved compositions.

the phreatomagmatic sequence above record two different events. The erosion of the top of the scoria deposit indicates that in the initial phase, dilute PDCs associated with the phreatomagmatic activity had an erosive behaviour capable of eroding the substrate in proximal areas. The following currents were in turn characterized by a depositional behaviour that led to the emplacement of the fully dilute PDC deposits. Such different behaviours are common and result from the intrinsic non-uniformity of dilute PDCs that can be erosional or depositional in different areas and/or at different times (Branney and Kokelaar, 2002).

The weakness of the interpretation associated with the end of FVS2 and beginning of the phreatomagmatic activity is increased by the presence of an unconformity that characterizes the phreatomagmatic sequence in proximal areas (Fig. 3h and i). This unconformity may record the intersection of PDCs with different directions (with erosion of the first), or alternatively, mark a temporal gap in the geological record.

In a first hypothesis, a transition of eruptive style from Strombolian to phreatomagmatic during the FVS2 eruption can be proposed, in which case all the phreatomagmatic products would be part of FVS2. However, this cannot account for an ~80 years of time interval between the scoria deposit and the dense PDC deposit at the top of the phreatomagmatic sequence, unless an internal separation between two episodes is considered. This, on the other hand, is very hard to distinguish in the

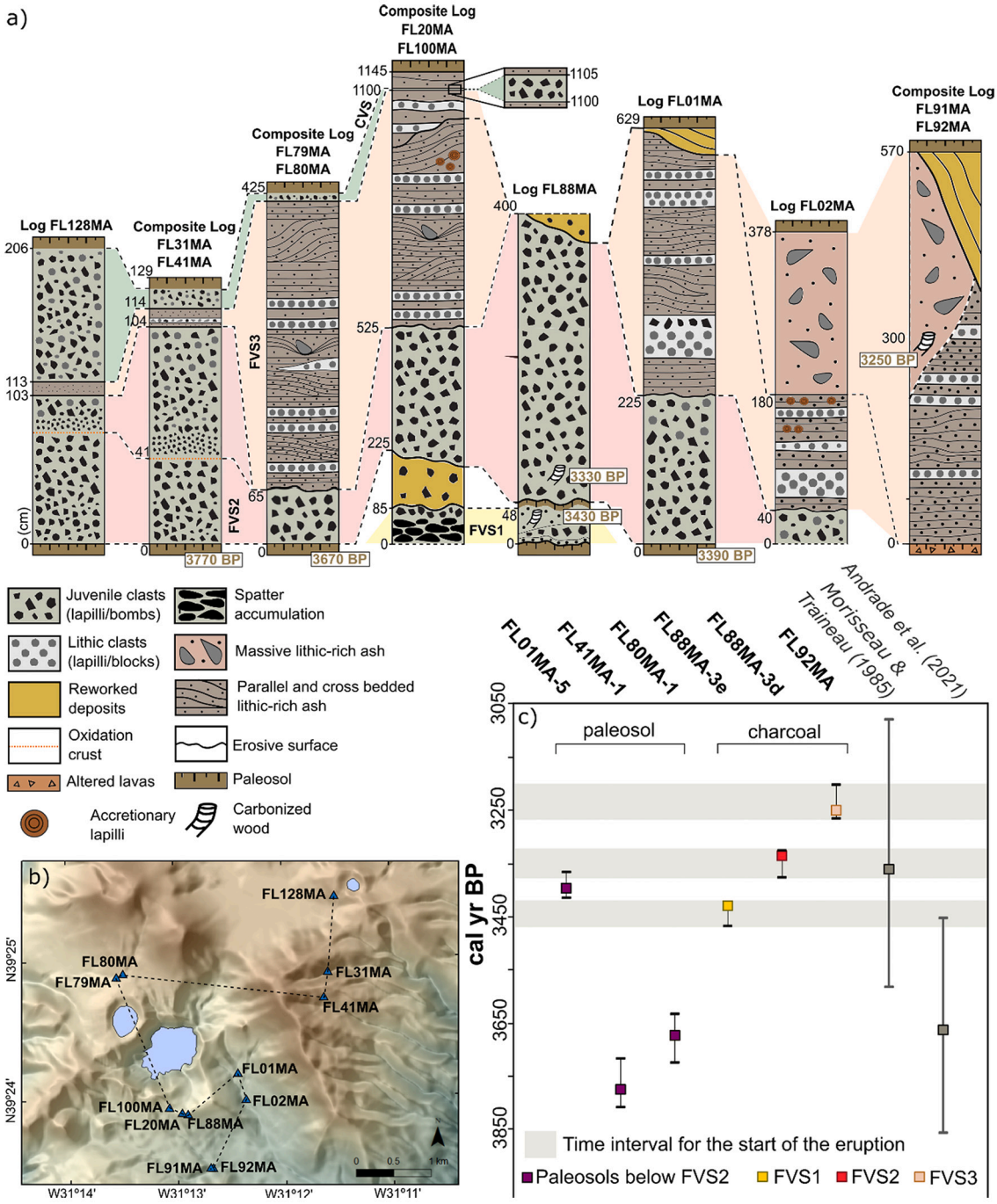

Fig. 6. a) Correlation panel of the main FVS sequences. Dashed lines correlate the different deposits and the shaded areas numerated from FVS1 to FVS3 identify the different volcanic eruptions. Scoriae identified by the green shaded area do not result from FVS eruptions but likely from Comprida Volcanic System (CVS). White boxes indicate the radiocarbon ages obtained for the volcanic deposits; b) location of the different volcanic sequences used for correlations, plotted over a digital elevation model of the area. Dashed line shows the spatial correlation between the different sequences. c) plot of the radiocarbon ages obtained (from paleosols and charcoal) for the different FVS eruptions and respective range of confidence. On the right side are plotted the ages and respective range of confidence attributed to FVS by Morisseau and Traineau (1985) and Andrade et al. (2021). (For interpretation of the references to colour in this figure legend, the reader is referred to the web version of this article.)

field. In a second hypothesis, we suggest that the FVS2 started as a Strombolian eruption and ended with phreatomagmatic activity. Subsequently, after a time break of ~80 years (recorded by the unconformity), a new purely phreatomagmatic eruption occurred. However, no paleosol was found in the middle of the phreatomagmatic sequence, something that would be expected in a humid environment like Flores (in comparison with the 5 cm thick paleosol below FSV2 that represents ~100 years). Nevertheless, it must be taken into account that the dilute PDCs associated with the new phreatomagmatic eruption, may have had an erosive behaviour capable of eroding a thin paleosol. In the absence of clear evidence to resolve this issue and to avoid erroneous interpretations, we assign the entire phreatomagmatic sequence to the FVS3 eruption (Fig. 6). Although the exact stratigraphic position of the FVS2-FVS3 boundary remains dubious, the current geomorphology of the maars and tuff rings, allow us to reconstruct the sequence of phreatomagmatic events that followed FVS1 and FVS2 magmatic

eruptions (Fig. 7).

The first phreatomagmatic phase(s) may have occurred at the SE and NE craters of the FVS. Both are intersected by the rim and tuff ring of Lagoa Funda maar (Fig. 7), indicating that the SE and NE craters were already present when the phreatomagmatic explosions that formed Lagoa Funda maar took place. The deposits associated with the NE crater were not observed in the field, but the rim of the SE crater is very-well exposed, showing the contact of the phreatomagmatic sequence with the scoria deposit below (e.g., field site FL20MA, Fig. 2a and c). The relative age between the NE and the SE craters is difficult to estimate. The NE crater is strongly eroded and therefore, it is reasonable to assume that it may have formed prior to the FVS. However, the NE crater works as a drainage basin of Lagoa Funda, which associated with the intense rainfall typically observed in the upland areas of Flores Island (Secretaria Regional do Ambiente e do Mar, 2012; Richter et al., 2022; Ritter et al., 2022), may explain the excavation of deep valleys.

The overlapping relationship of the different craters of the FVS indicates that the formation of the Lagoa Funda maar occurred after the NE and SE craters were formed. Lagoa Funda maar must have been the main vent of the FVS, involving a highly explosive eruption that displaced a large amount of material. Simultaneous ash fallout and fully dilute PDCs associated with phreatomagmatic activity led to the deposition of the bedded lithic-rich ash deposits over a large area. At a later phase, hot high particle concentration granular fluid-based currents (dense PDCs) were generated (one of them dated at 3250 cal yr BP; Table 1 and Fig. 6) likely related to the collapse of the eruptive column.

The final stage of the phreatomagmatic activity was marked by the formation of the small tuff ring that now hosts Lagoa Rasa (Fig. 7). We interpret this as the last event of the FVS based on geomorphological relations, otherwise the large volume of material produced during the formation of Lagoa Funda maar would have completely buried Rasa's shallow crater. The alignment of the SE crater, Lagoa Funda maar and Lagoa Rasa tuff ring suggests a dyke intrusion, which must have progressed along an eruptive fissure from SE to NW.

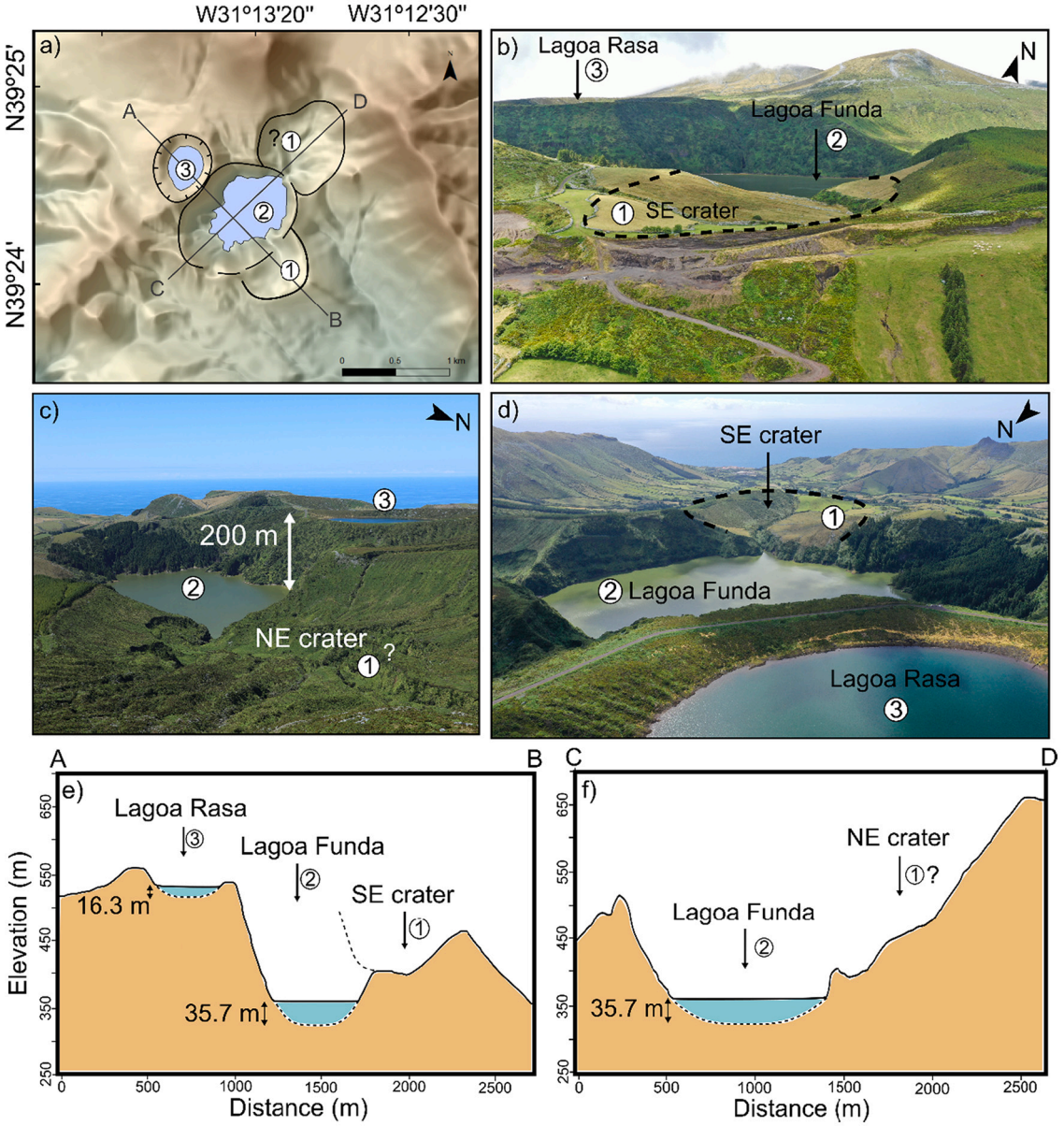

Fig. 7. Geometric relationships between the different craters of FVS. A) Digital elevation model with a detailed view of FVS showing the different craters and their interpreted chronological order of formation, 1 is the oldest and 3 the most recent. b-d) photographs with different views of the geometric relationships between the craters; e) NW-SE terrain profile of FVS; f) SW-NE terrain profile of FVS.

The phreatomagmatic sequence contains large amounts of lithic fragments, ranging in size from fine lapilli to blocks, including clasts of trachytic compositions (Fig. 5a). This suggests strong fragmentation and excavation of the country rocks, of Pleistocene age belonging to the Lower Unit of the Upper Complex (Azevedo and Portugal Ferreira, 2006), where the phreatomagmatic activity of the FVS occurred. At the top of the FVS pyroclastic sequence, a thin scoria fall unit is present. Due to its spatial distribution with deposit thickness increasing northwards, this scoria unit was associated with eruptions sourced from CVS (Fig. 6). The CVS goes beyond the goals of this work and therefore this unit is not discussed in detail here.

5.2. Reconstruction of eruption dispersal and source parameters

In this section, we reconstruct the dispersal of the products of the FVS eruptions and estimate eruption source parameters. The FVS1 Strombolian eruption seems to have had a very reduced dispersal as the products (scoriaceous ash and spatter) crop out only in the quarry located on the rim of the SE crater and were not found in Lagoa da Lomba lacustrine record (see Andrade et al., 2021 for details). Due to the limited outcrops and consequent lack of data for FVS1 it was not possible to estimate eruption parameters for this unit.

5.2.1. FVS2 eruption

The FVS2 Strombolian eruption was marked by a brief unsteadiness of the eruption column (and eventually a small shift in wind conditions) that is recorded by a grain size variation in the scoria deposit. Thus, we reconstructed separate isopach and isopleth maps for the tephra beds below (FVS2a) and above (FSV2b) this granulometric variation. It is worth noting that such an internal grain size variation is not always present in the FVS2 deposits and when geochemical data were not available, it was not possible to separate FVS2a from FVS2b. For that reason, some of the data points were used to draw isopachs and isopleths of the total FVS2 deposit but were not used for the subunits FVS2a and

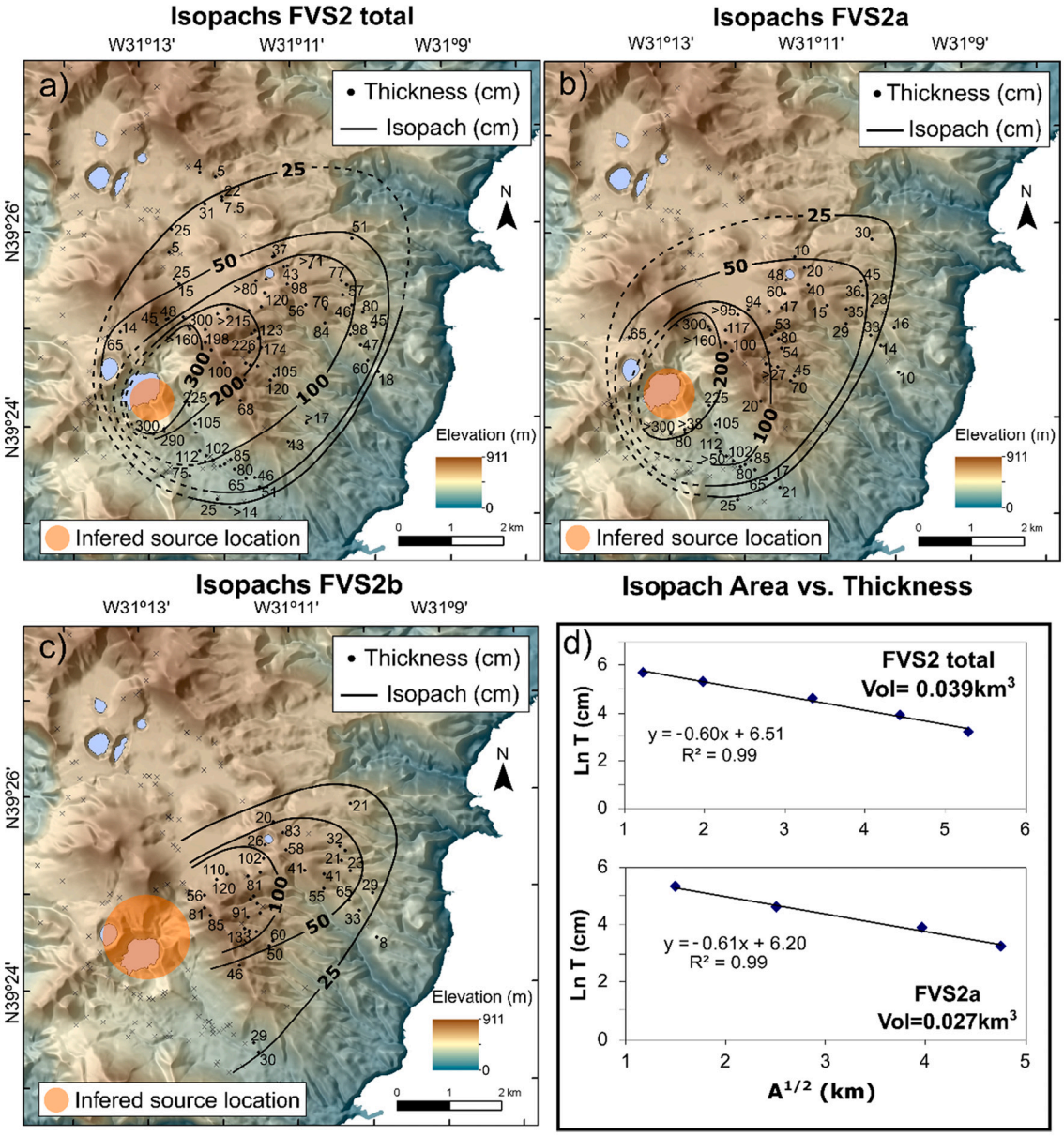

Fig. 8. Isopach map of a) FVS2 total deposit, b) FVS2 tephra below the grain size variation (FVS2a) and, c) FVS2 tephra above the grain size variation (FVS2b). Grey crosses represent field sites where the deposit is absent. d) log of thickness vs. square root of area diagrams for the total (upper) FVS2 deposit and before the grain size change (bottom).

FVS2b (Figs. 8 and 9).

Isopach and isopleth maps show a single axis of dispersal oriented to NE, indicating that the wind was mainly blowing from SW during FVS2 eruption (Figs. 8 and 9). This dispersal direction is consistent with the current wind pattern for the Azores region, which is dominated by westerly-blowing winds (Pimentel et al., 2006; Gaspar et al., 2015). Paleowind directions reconstructed from tephra dispersal on São Miguel Island (Azores) show the same prevalent westerly-blowing winds over the last 5000 years (Booth et al., 1978). FVS2 isopachs are overall regularly spaced, suggesting a good exponential thinning of the deposit with distance from the source, which is also illustrated by the single straight line between data points in the ln (thickness) vs. square root (isopach area) diagrams (Fig. 8d). However, isopachs and isopleths show some near-vent deviations (Figs. 8 and 9), eventually reflecting the influence of ballistics and/or the lack of data points in the N, NW, and W areas of FVS.

The total FVS2 scoria fall deposit covers an area of 28.07 km^2 within the 25-cm isopach and yields a proximal volume of 0.039 km^3 (Table 1). However, it is well known that estimating tephra volumes on islands is challenging as the deposits are often incompletely preserved due to the reduced subaerial area of deposition. It is therefore reasonable to consider that a significant, but unknown, portion of pyroclastic material is deposited offshore, as commonly reported for other explosive eruptions on small islands (e.g., Andronico and Pistolesi, 2010; Pimentel et al., 2015, 2021; Kueppers et al., 2019). In the case of Flores, and as it happens in tropical and subtropical climates with strong winds and/or intense rainfall regimes, this is aggravated by the high *syn-* and post-depositional reworking of subaerial exposures (Bolós et al., 2021), and thus the estimates presented here must be considered as minimum erupted volumes. The resulting 0.039 km^3 total volume of FVS2 eruption corresponds to an event with a volcanic explosivity index of 3 (VEI; Newhall and Self, 1982). An erupted mass of 3.064×10^{10} kg was calculated considering a tephra density of 776 kg/m^3 (see methods for details), corresponding to a dense rock equivalent (DRE) volume of 0.011 km^3 (using a trachybasaltic magma density of 2800 kg/m^3 given by Pimentel et al., 2016). FVS2 classifies as an event with an eruption magnitude of 3.5 (Table 1).

The subunit below the grain size variation (FSV2a) comprises most of the erupted material, with an estimated volume of 0.027 km^3 and an erupted mass of 2.006×10^{10} kg, considering a tephra density of 755 kg/m^3 (Fig. 8, Table 1). Due to the lack of information on the N, S and W sectors, it was not possible to close the isopachs for FVS2b and, therefore, its volume was not estimated using the method of Pyle (1989) modified by Fierstein and Nathenson (1992). Nevertheless, an indicative volume of 0.012 km^3 was obtained for FVS2b by subtracting the volume of FVS2a from the total eruption.

Although incomplete, isopachs of FVS2b show the same dispersal orientation as FVS2a and total FVS2 (Fig. 8). For that reason, we consider that the internal grain size variation in the FVS2 deposit is related either to changes in the eruptive dynamics (e.g., decrease of eruption rate) and/or wind speed, rather than a change in the wind direction. Overall, the orientation of the isopleths (Fig. 9) is consistent with the orientation of the isopachs (Fig. 8), with average maximum size of lithics and juveniles decreasing north-eastwards. Despite being a Strombolian-style eruption, FVS2 was a large event and developed an eruption column that was strongly dispersed by the wind, as evidenced by the orientation of isopach and isopleth maps. Although the requirements for applying the Carey and Sparks (1986) method were not optimal, we plotted the maximum downwind and crosswind ranges of the 3.2 cm lithic isopleth from the total FVS2 deposit to estimate a maximum column height. Based on that, we obtained an eruption column height of ~9.4 km and wind speeds of 10 to 20 m/s (36–72 km/h; Fig. 9f). Such column height is close to the top limit of Strombolian eruptions (<10 km; Cas and Wright, 1987), which indicates that FVS2 eruption must have been a violent Strombolian event, similar to those recorded at Tecolote (Zawacki et al., 2019), Okmok (Wong and Larsen, 2010), Parícutin (Pioli et al., 2008) or Vesuvius (Arrighi et al., 2001). Considering a column height of 9.4 km, we estimate a mass eruption rate of 1.03×10^6 kg/s, which corresponds to an intensity of 9 (Table 2). Lithic clasts are very rare below the grain size variation (FVS2a) and, therefore, only juvenile isopleths were reconstructed (Fig. 9e). The presence of lithics increases at FVS2b but the scarcity of data points on the N, S and W sectors does not allow the reconstruction of complete isopleths (Fig. 9c and d). For those reasons, eruption column height and related parameters were only estimated for the total FVS2 deposit. All eruption source parameters are summarized in Table 2.

5.2.2. FVS3 eruption

The FVS3 phreatomagmatic eruption (which may include the final stage of FVS2, as discussed in the Section 5.2.1) was characterized by pulsating activity that produced short-lived unstable eruption columns generating widespread ash fallout and fully dilute PDCs. The concomitance of different transport and depositional mechanisms does not allow the discrimination of the pyroclastic material deposited by each process. In proximal areas, pyroclastic deposition was dominated by the emplacement of dilute PDCs. The approximately concentric deposit thickness variation from the source area (Fig. 10) suggests discrete fountain collapse episodes forming single pulses of dilute PDCs radially flowing in different directions, or, alternatively, a more intense production of steam at the vent, which generated fully dilute PDCs.

In more distal areas, the deposit distribution resembles the isopach maps for FSV2 scoria fall deposits, demonstrating that ash fallout was dominant and being controlled by the prevailing wind direction blowing from SW (Fig. 10). The volume of the phreatomagmatic material was estimated by multiplying the area of each polygon by its average thickness, yielding a volume in the order of 0.030 km^3.

The emplacement of dense PDC deposits at the final stage of FVS3 eruption was strongly controlled by topography, with the pyroclastic material being deposited mostly on Ribeira das Lajes and Ribeira Seca valleys (Fig. 10). In contrast to what occurs at Ribeira das Lajes, where the dense PDC deposit crops out along the extension of the valley, at Ribeira Seca the deposit is apparently absent in the most proximal areas, suggesting post-eruptive erosion or current bypass (i.e., passage of a PDC without deposition; Brown and Branney, 2004) in the steep proximal slopes. The high particle concentration nature of these currents suggests generation from the total collapse of the eruption column. Such collapse likely resulted from the widening of the conduit due to continuous excavation and erosion of the conduit walls leading to a decrease in the discharge rate and subsequent unsustained eruption column. The mapped distribution of the dense PDC deposits is restricted to the two above mentioned valleys (Fig. 10) with an estimated volume of only 6×10^{-4} km^3.

5.3. Eruptive style transition

The FVS pyroclastic sequence records a clear change in eruptive style from the purely magmatic Strombolian activity of FVS1 and FVS2 to the phreatomagmatic activity that characterizes FVS3. However, due to the difficulty in determining the exact moment when the eruptive style transition occurred, two scenarios must be discussed:

1) *FVS2 is purely Strombolian and all phreatomagmatic activity is attributed to FVS3.* In this case, magmatic and phreatomagmatic activity must have occurred ~80 years apart. Since water disposal at inland areas is strongly dependent on climatic factors, long-term high precipitation may have contributed to increase groundwater availability on Flores central upland area, allowing for optimum magma/water ratios to produce phreatomagmatism. Kereszturi et al. (2011) found a clear correlation between climate and style of volcanism at the Bakony-Balaton highland volcanic field (western Hungary), with scoria cones being formed during drier conditions and maars and tuff rings during more humid conditions. Such relation can be difficult to

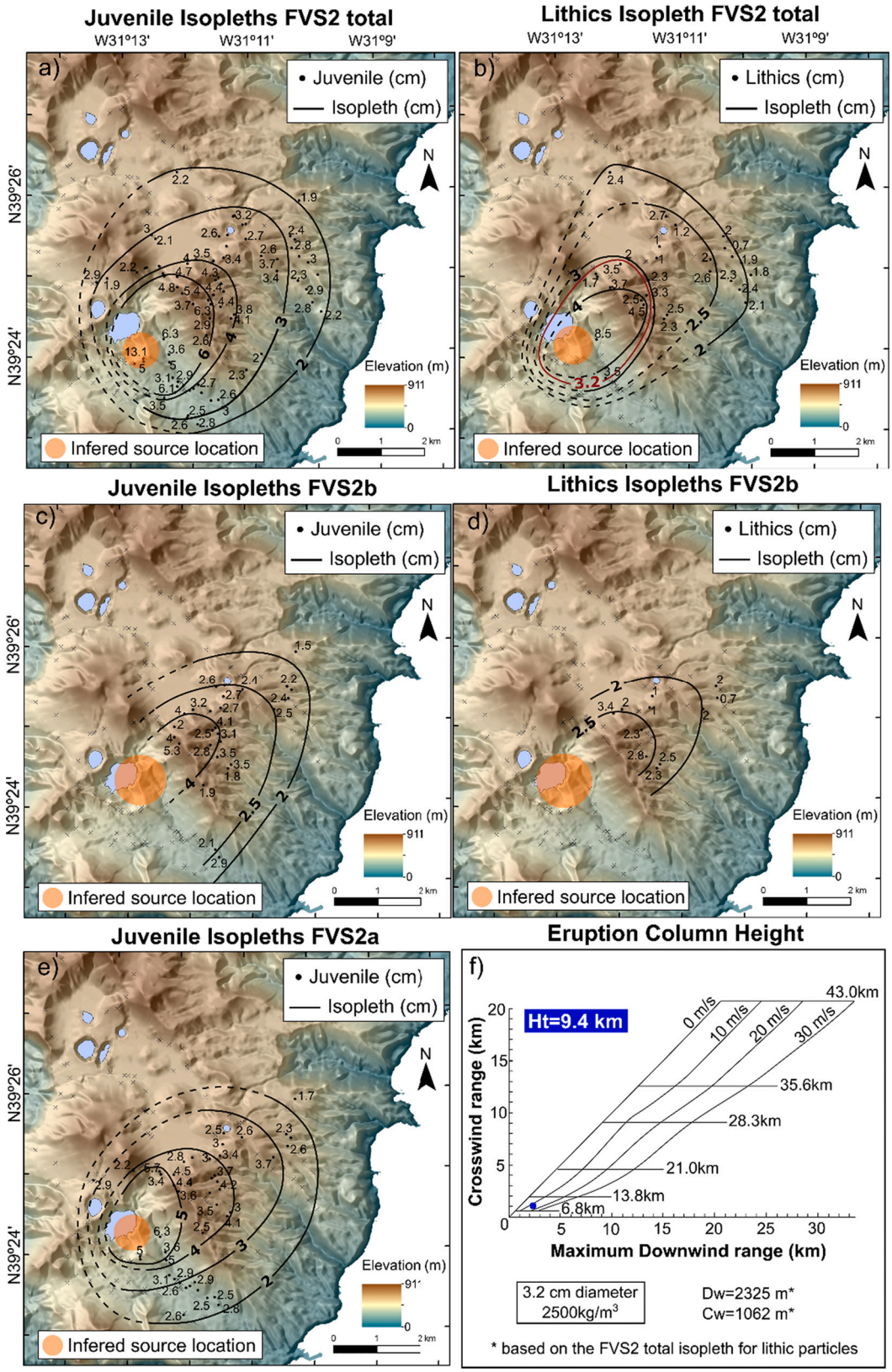

Fig. 9. Isopleth map of FVS2 deposit for a) juvenile and b) lithic clasts; The 3.2 isopleth in red was used to calculate the eruption column height following Carey & Sparks, (1986); c) Isopleth map of FVS2 deposits above the grain size variation (FVS2b) for juvenile and d) lithic clasts; e) Isopleth map of FVS2 deposit below the grain size variation (FVS2a) for juvenile clasts; Grey crosses represent field sites where the deposit is absent; f) Crosswind range vs. downwind range diagram for 3.2 cm clast diameter and 2500 kg/m^3 density based on Carey & Sparks, (1986). (For interpretation of the references to colour in this figure legend, the reader is referred to the web version of this article.)

Table 2
Summary of the source parameters of FVS2 eruption.

Parameters	FVS2 total	FVS2a	FVS2b
Proximal volume (km^3)[1]	0.039	0.027	0.012*
Volcanic explosivity index (VEI)[2]	3	3	–
Erupted mass ($x10^{10}$ kg)[3]	3.064	2.006	–
Magnitude[4]	3.5	3.3	–
Dense rock equivalent (DRE) volume (km^3)[5]	0.011	0.070	–
Eruption column height (km)[6]	9.4	–	–
Mass eruption rate ($x10^6$ kg/s)[7]	1.03	–	–
Intensity[8]	9.0	–	–

(*) FVS2b volume was calculated by subtracting the volume of FVS2a to the FVS2 total.
[1] After Pyle (1989) modified by Fierstein and Nathenson (1992).
[2] After Newhall and Self (1982).
[3] Using average tephra density of 776 kg/m^3 (FVS2 total) and 755 kg/m^3 (FVS2a).
[4] After Pyle (2000).
[5] Using average tephra density and trachybasalt magma density of 2800 kg/m^3.
[6] After Carey and Sparks (1986).
[7] After Wilson and Walker (1987) modified by Costantini et al., 2009.
[8] After Pyle (2000).

evaluate in areas where volcanism is dormant for long periods as it is the case for Flores Island. However, in future studies it would be worth investigating a possible relationship between climatic conditions and eruptive styles at Flores, using proxy-based climate reconstructions obtained from sedimentary records.

2) *FVS2 eruption changed from Strombolian to phreatomagmatic.* In this scenario, the initial high eruption rate and magma pressure in the conduit may have inhibited groundwater to enter the plumbing system. This would correspond to the purely magmatic scoria fall deposit that characterizes the beginning of FVS2 eruption (i.e., the FVS2a tephra). A brief decrease in the eruption rate may have allowed for groundwater to gradually enter the system, which enhanced fragmentation and excavation of the conduit rocks. This is seen in the field by the increase of lithics in the FVS2b tephra. At some point magma pressure may have fallen below a certain threshold, possibly because of the widening of the conduit, allowing for large amounts of groundwater to enter the plumbing system, resulting in the sudden transition from Strombolian to phreatomagmatic activity (Houghton and Schmincke, 1989; Gutman, 2002). Similar transitions from "dry" to "wet" conditions are commonly described for mafic volcanoes where Strombolian activity is followed by phreatomagmatism (Gisbert et al., 2009; Di Traglia et al., 2009; Saucedo et al., 2017; Zanon and Viveiros, 2019; Geshi et al., 2019; Pedrazzi et al., 2022). In some cases, a final purely magmatic phase is described at the end of the eruption. This apparent dry out of the system is usually attributed to the exhausting of the aquifers. In the case of FVS there is an irreversible change from Strombolian to phreatomagmatic activity, meaning that there was enough groundwater to fuel phreatomagmatism until the end of the eruption, which is unsurprising in a context like Flores, which represents a hydraulically-charged volcanic edifice.

Independently of the scenario considered, the phreatomagmatism of FVS produced a complex geomorphology of maars and tuff rings. The different types of volcanic structures suggest the occurrence of different magma/water ratios during the period of phreatomagmatic activity. Maar-type explosions are typically favoured by a magma/water ratio of 3:1, whereas formation of tuff rings is favoured by a ratio of 1:1 (Lorenz, 1986). Accordingly, Lagoa Funda maar might have been formed when magma eruption rates were higher and the SE crater and Lagoa Rasa tuff rings when magma eruption rates were lower compared to the amount of water entering the system.

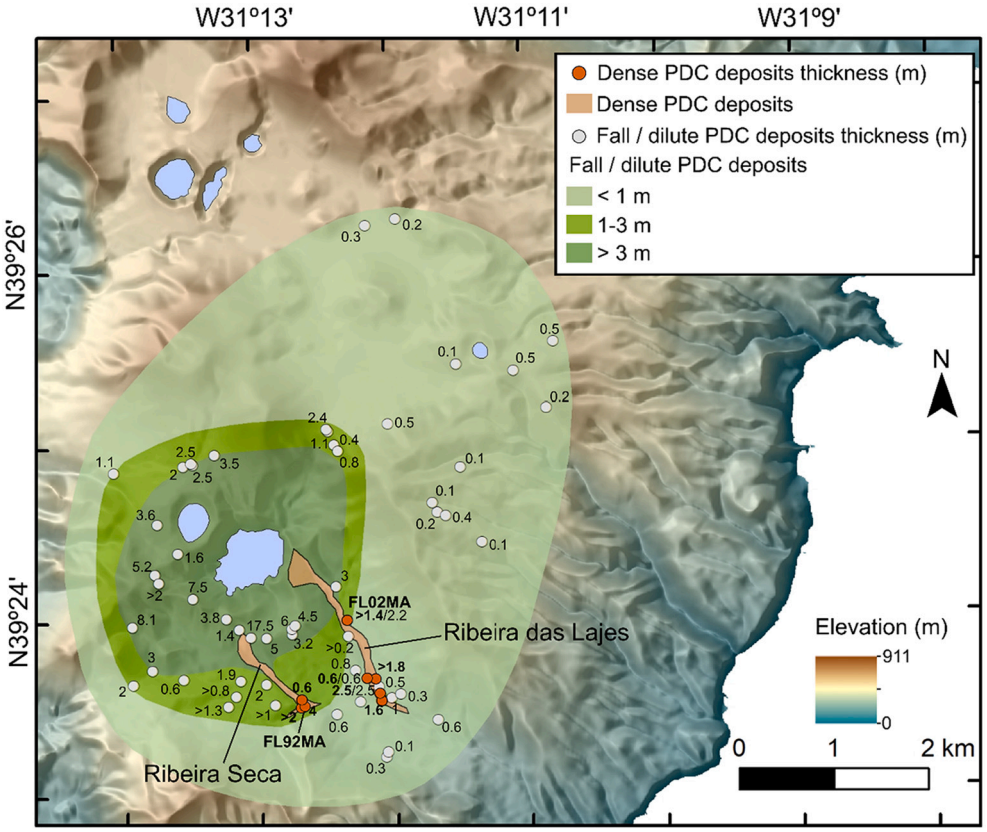

Fig. 10. Map of phreatomagmatic products of FVS3 eruption. White circles indicate the thickness of the bedded lithic-rich sequence (intercalation of fully dilute PDC and fall deposits) and the green shaded areas represent its variation. Orange circles indicate the thickness of dense PDC deposits, and the shaded areas represent its distribution. The location of the deposits shown in Fig. 4 is highlighted in bold. (For interpretation of the references to colour in this figure legend, the reader is referred to the web version of this article.)

6. Conclusions

Stratigraphy of the FVS shows that its eruptive history was marked by at least three different volcanic eruptions spaced by time intervals of ~100 yr. The first (3430 cal yr BP) was a small Strombolian eruption whose products are limited to a small area south of the FVS; the second (3330 cal yr BP) started with a VEI 3 Strombolian eruption that dispersed tephras along the entire central area of the island and may have ended with violent phreatomagmatic explosions; the third eruption (3250 cal yr BP) was exclusively phreatomagmatic, characterized by violent explosions, and ended with the generation of dense PDCs.

The new data show that eruptions of the FVS were more recurrent and lasted longer than previously reported. Instead of a single event (Morisseau and Traineau, 1985; Azevedo and Portugal Ferreira, 2006; Andrade et al., 2021), we demonstrate that the FVS experienced multiple eruptions over a period comprising almost 200 yr. We also show that a variety of eruptive styles occurred at the FVS, ranging from small Strombolian eruptions to violent Strombolian and phreatomagmatic events; this diversity has clear hazard implications, which are worth exploring in the future.

Due to the relatively small size of the eruptions and long periods of inactivity, monogenetic volcanoes, such as those from Flores, are usually seen as non-hazardous (Pedrazzi et al., 2022). In fact, the volcanic history of Flores has been marked by long periods of quiescence, which associated with the absence of historical eruptions and its location in a relatively stable tectonic setting can create a false sense of safety. The study of the past activity is thus crucial to predict realistic scenarios of future volcanic events. Moreover, since magma/water interactions, may give rise to activity that is more explosive and less predictable in intensity and duration (Clarke et al., 2009; Pedrazzi et al., 2022), a good understanding of the subsurface geology of the volcanic systems, including the distribution and hydraulic characteristic of the aquifers, would be essential for a complete and more precise assessment of volcanic hazards at Flores Island.

Supplementary data to this article can be found online at https://doi.org/10.1016/j.jvolgeores.2022.107706.

Funding

This work was funded by the Portuguese Fundação para a Ciência e a Tecnologia (FCT) I.P./MCTES through national funds *(PIDDAC) – UIDB/50019/2020 - and project IF/01641/2015 MEGAWAVE.*. MA is funded by FCT through her doctoral grant (SFRH/BD/138261/2018). AH is funded by the Spanish Ministry of Science and Innovation through the Ramón y Cajal Scheme [RYC2020-029253-I].

Credit author statement

Mariana Andrade: field work, sample preparation, glass shards geochemical analysis and subsequent data processing, investigation, conceptualization, writing – original draft – review & editing.

Adriano Pimentel: field work, conceptualization, discussion of the results, writing – review & editing, supervision.

Ricardo Ramalho: field work, conceptualization, discussion of the results, writing – review & editing, supervision, field funding.

Steffen Kutterolf: sample preparation, glass shards geochemical analysis and subsequent data processing, discussion of the results, writing – review & editing.

Armand Hernández: field work, discussion of the results, writing – review & editing, supervision.

Declaration of Competing interest

The authors declare that they have no known competing financial interests or personal relationships that could have appeared to influence the work reported in this paper.

Data availability

Data will be made available on request.

Acknowledgements

We acknowledge GEOMAR Helmholtz Centre for providing the facilities and technical support during the geochemical analyses. We thank M. Antunes at Secretaria Regional do Turismo e Transportes for providing the digital altimetric database used in this study. We also acknowledge Serviços Florestais das Flores e Corvo as well as Câmara Municipal das Lajes das Flores, for their support in field logistics and access to some of the outcrops. We thank Dario Pedrazzi and an anonymous reviewer for their constructive comments and José Luis Macías for his thoughtful review and editorial handling.

References

Andrade, C., Cruz, J., Viveiros, F., Coutinho, R., 2019. CO2 Flux from Volcanic Lakes in the Western Group of the Azores Archipelago (Portugal). Water 11 (3), 599. https://doi.org/10.3390/w11030599.

Andrade, M., Ramalho, R.S., Pimentel, A., Hernández, A., Kutterolf, S., Sáez, A., Benavente, M., Raposeiro, P.M., Giralt, S., 2021. Unraveling the Holocene Eruptive history of Flores Island (Azores) through the Analysis of Lacustrine Sedimentary Records. Front. Earth Sci. 889 https://doi.org/10.3389/feart.2021.738178.

Andronico, D., Pistolesi, M., 2010. The November 2009 Paroxysmal explosions at Stromboli. Journal of Volcanology Geothermal Research 196, 120–125. https://doi.org/10.1016/j.jvolgeores.2010.06.005.

Arrighi, S., Principe, C., Rosi, M., 2001. Violent strombolian and subplinian eruptions at Vesuvius during post-1631 activity. Bull. Volcanol. 63 (2), 126–150. https://doi.org/10.1007/s004450100130.

Azevedo, J.M.M., Portugal Ferreira, M., 1999. Volcanic gaps and subaerial records of palaeo-sea-levels on Flores Island (Azores): tectonic and morphological implications. J. Geodyn. 28 (2–3), 117–129. https://doi.org/10.1016/S0264-3707(98)00032-5.

Azevedo, J.M.M., Portugal Ferreira, M.R., 2006. The Volcanotectonic Evolution of Flores Island, Azores (Portugal). J. Volcanol. Geotherm. Res. 156 (1–2), 90–102. https://doi.org/10.1016/j.jvolgeores.2006.03.011.

Azevedo, J.M.M., Ferreira, M.R., Martins, J.Á., 1991. The Emergent Volcanism of Flores Islands, Azores (Portugal). Arquipélago-Life and Earth Sciences 9, 37–46.

Barberi, F., Cioni, R., Rosi, M., Santacroce, R., Sbrana, A., Vecci, R., 1989. Magmatic and phreatomagmatic phases in explosive eruptions of Vesuvius as deduced by grain-size and component analysis of the pyroclastic deposits. J. Volcanol. Geotherm. Res. 38 (3–4), 287–307. https://doi.org/10.1016/0377-0273(89)90044-9.

Barker, A.K., Troll, V.R., Carracedo, J.C., Nicholls, P.A., 2015. The magma plumbing system for the 1971 Teneguía eruption on La Palma, Canary Islands. Contrib. Mineral. Petrol. 170 (5), 1–21. https://doi.org/10.1007/s00410-015-1207-7.

Bolós, X., Macias, J.L., Ocampo-Díaz, Y.Z.E., Tinoco, C., 2021. Implications of reworking processes on tephra distribution during volcanic eruptions: the case of Parícutin (1943–1952, western Mexico). Earth Surf. Process. Landf. 46 (15), 3143–3157. https://doi.org/10.1002/esp.5222.

Booth, B., Croasdale, R., Walker, G.P.L., 1978. A quantitative study of five thousand years of volcanism on Sao Miguel, Azores. Philosophical Transactions of the Royal Society of London. Series A, Mathematical and Physical Sciences 288 (1352), 271–319. https://doi.org/10.1098/rsta.1978.0018.

Branney, M.J., Kokelaar, P., 2002. Pyroclastic Density Currents and the Sedimentation of Ignimbrites. Geological Society of London, Mems 27, 152. https://doi.org/10.1144/GSL.MEM.2003.027.

Brown, R.J., Branney, M.J., 2004. Bypassing and diachronous deposition from density currents: evidence from a giant regressive bed form in the Poris ignimbrite, Tenerife. Canary Islands. Geology 32 (5), 445–448. https://doi.org/10.1130/G20188.1.

Carey, S., Sparks, R.S.J., 1986. Quantitative models of the fallout and dispersal of tephra from volcanic eruption columns. Bull. Volcanol. 48 (2), 109–125. https://doi.org/10.1007/BF01046546.

Cas, R.A.F., Wright, J.V., 1987. Volcanic Successions: Ancient and Modern. Allen and Union, London.

Chester, D., Duncan, A., Coutinho, R., Wallenstein, N., Branca, S., 2017. Communicating Information on Eruptions and their Impacts from the Earliest Times until the late Twentieth century. In: Observing the Volcano World. Springer, Cham, pp. 419–443. https://doi.org/10.1007/11157_2016_30.

Clarke, H., Troll, V.R., Carracedo, J.C., 2009. Phreatomagmatic to strombolian eruptive activity of basaltic cinder cones: Montana Los Erales, Tenerife, Canary Islands. J. Volcanol. Geotherm. Res. 180 (2–4), 225–245. https://doi.org/10.1016/j.jvolgeores.2008.11.014.

Connor, C.B., Conway, F.M., 2000. Basaltic volcanic fields. Encyclopedia of volcanoes 1, 331–343.

Costantini, L., Bonadonna, C., Houghton, B.F., Wehrmann, H., 2009. New physical characterization of the Fontana Lapilli basaltic Plinian eruption, Nicaragua. Bulletin of Volcanology 71, 337. https://doi.org/10.1007/s00445-008-0227-9.

Di Traglia, F., Cimarelli, C., De Rita, D., Torrente, D.G., 2009. Changing eruptive styles in basaltic explosive volcanism: examples from Croscat complex scoria cone, Garrotxa

Volcanic Field (NE Iberian Peninsula). J. Volcanol. Geotherm. Res. 180 (2–4), 89–109. https://doi.org/10.1016/j.jvolgeores.2008.10.020.
EMODnet Bathymetry Consortium, 2018. EMODnet Digital Bathymetry (DTM 2018). Hydrographic and Oceanographic Service of the Navy (SHOM), France. https://doi.org/10.12770/18ff0d48-b203-4a65-94a9-5fd8b0ec35f6.
Fierstein, J., Nathenson, M., 1992. Another look at the calculation of fallout tephra volumes. Bull. Volcanol. 54 (2), 156–167. https://doi.org/10.1007/BF00278005.
Gaspar, J.L., Queiroz, G., Ferreira, T., Medeiros, A.R., Goulart, C., Medeiros, J., 2015. Earthquakes and volcanic eruptions in the Azores region: geodynamic implications from major historical events and instrumental seismicity. Geological Society, London, Memoirs 44 (1), 33–49. https://doi.org/10.1144/M44.4.
Genske, F.S., Beier, C., Stracke, A., Turner, S.P., Pearson, N.J., Hauff, F., Scaefer, B.F., Haase, K.M., 2016. Comparing the Nature of the Western and Eastern Azores Mantle. Geochim. Cosmochim. Acta 172, 76–92. https://doi.org/10.1016/j.gca.2015.08.019.
Gente, P., Dyment, J.R.M., Maia, M., Goslin, J., 2003. Geochem. Geophys. Geosyst. 4 (10) https://doi.org/10.1029/2003GC000527.
Geshi, N., Németh, K., Noguchi, R., Oikawa, T., 2019. Shift from magmatic to phreatomagmatic explosions controlled by the lateral evolution of a feeder dike in the Suoana-Kazahaya eruption, Miyakejima Volcano, Japan. Earth Planet. Sci. Lett. 511, 177–189. https://doi.org/10.1016/j.epsl.2019.01.038.
Gisbert, G., Gimeno, D., Fernandez-Turiel, J.L., 2009. Eruptive mechanisms of the Puig De La Garrinada volcano (Olot, Garrotxa volcanic field, Northeastern Spain): a methodological study based on proximal pyroclastic deposits. J. Volcanol. Geotherm. Res. 180 (2–4), 259–276. https://doi.org/10.1016/j.jvolgeores.2008.12.018.
Gutmann, J.T., 2002. Strombolian and effusive activity as precursors to phreatomagmatism: eruptive sequence at maars of the Pinacate volcanic field, Sonora, Mexico. J. Volcanol. Geotherm. Res. 113 (1–2), 345–356. https://doi.org/10.1016/S0377-0273(01)00265-7.
Hildenbrand, A., Marques, F.O., Catalão, J., 2018. Large-scale mass wasting on small volcanic islands revealed by the study of Flores Island (Azores). Sci. Rep. 8 (1), 1–11. https://doi.org/10.1038/s41598-018-32253-0.
Houghton, B.F., Nairn, I.A., 1991. The 1976–1982 Strombolian and phreatomagmatic eruptions of White Island, New Zealand: eruptive and depositional mechanisms at a 'wet' volcano. Bull. Volcanol. 54 (1), 25–49. https://doi.org/10.1007/BF00278204.
Houghton, B.F., Schmincke, H.U., 1989. Rothenberg scoria cone, East Eifel: a complex Strombolian and phreatomagmatic volcano. Bull. Volcanol. 52 (1), 28–48. https://doi.org/10.1007/BF00641385.
Hunt, J.B., Hill, P.G., 2001. Tephrological implications of beam size—sample-size effects in electron microprobe analysis of glass shards. Journal of Quaternary Science: Published for the Quaternary Research Association 16 (2), 105–117. https://doi.org/10.1002/jqs.571.
Jarosewich, E., Nelen, J.A., Norberg, J.A., 1980. Reference samples for electron microprobe analysis. Geostand. Newslett. 4 (1), 43–47. https://doi.org/10.1111/j.1751-908X.1980.tb00273.x.
Kereszturi, G., Németh, K., Csillag, G., Balogh, K., Kovács, J., 2011. The role of external environmental factors in changing eruption styles of monogenetic volcanoes in a Mio/Pleistocene continental volcanic field in western Hungary. J. Volcanol. Geotherm. Res. 201 (1–4), 227–240. https://doi.org/10.1016/j.jvolgeores.2010.08.018.
Klügel, A., Hoernle, K.A., Schmincke, H.U., White, J.D.L., 2000. The chemically zoned 1949 eruption on La Palma (Canary Islands): petrologic evolution and magma supply dynamics of a rift- zone eruption. Journal of Geophysical Research: Solid Earth 105 (B3), 5997–6016. https://doi.org/10.1029/1999JB900334.
Kueppers, U., Pimentel, A., Ellis, B., Forni, F., Neukampf, J., Pacheco, J., Perugini, D., Queiroz, G., 2019. Biased volcanic hazard assessment due to incomplete eruption records on ocean islands: an example of Sete Cidades Volcano. Azores. Frontiers in Earth Science 7, 122. https://doi.org/10.3389/feart.2019.00122.
Kutterolf, S., Freundt, A., Burkert, C., 2011. Eruptive history and magmatic evolution of the 1.9 kyr Plinian dacitic Chiltepe Tephra from Apoyeque volcano in west-Central Nicaragua. Bull. Volcanol. 73 (7), 811–831. https://doi.org/10.1007/s00445-011-0457-0.
Latutrie, B., Ross, P.S., 2020. Phreatomagmatic vs magmatic eruptive styles in maar-diatremes: a case study at Twin Peaks, Hopi Buttes volcanic field, Navajo Nation, Arizona. Bulletin of Volcanology 82 (3), 1–25. https://doi.org/10.1007/s00445-020-1365-y.
Le Bas, M.J., Le Maitre, R.W., Streckeisen, A., Zanettin, B., 1986. A chemical classification of volcanic rocks based on the total alkali-silica diagram. J. Petrol. 27 (3), 745–750. https://doi.org/10.1093/petrology/27.3.745.
Lorenz, V., 1986. On the growth of maars and diatremes and its relevance to the formation of tuff rings. Bull. Volcanol. 48 (5), 265–274. https://doi.org/10.1007/BF01081755.
Martí, J., Planagumà, L., Geyer, A., Canal, E., Pedrazzi, D., 2011. Complex interaction between Strombolian and phreatomagmatic eruptions in the Quaternary monogenetic volcanism of the Catalan Volcanic Zone (NE of Spain). J. Volcanol. Geotherm. Res. 201 (1–4), 178–193. https://doi.org/10.1016/j.jvolgeores.2010.12.009.
Morisseau, M., Traineau, H., 1985. Mise en évidence d'une activité hydromagmatique holocène sur l'île de Flores (Açores). Comptes rendus de l'Académie des sciences. Série 2, Mécanique, Physique, Chimie, Sciences de l'univers. Sci. Terre 301 (18), 1309–1314.
Németh, K., 2010. Monogenetic volcanic fields: Origin, sedimentary record, and relationship with polygenetic volcanism. In: What is a Volcano? GSA Special Paper, vol. 470, p. 43.
Németh, K., Cronin, S.J., Smith, I.E., Agustin Flores, J., 2012. Amplified hazard of small-volume monogenetic eruptions due to environmental controls, Orakei Basin, Auckland Volcanic Field. New Zealand. Bulletin of Volcanology 74 (9), 2121–2137. https://doi.org/10.1007/s00445-012-0653-6.
Newhall, C.G., Self, S., 1982. The volcanic explosivity index (VEI): an estimate of explosive magnitude for historical volcanism. Journal of Geophysical Research: Oceans 87 (C2), 1231–1238. https://doi.org/10.1029/JC087iC02p01231.
Pedrazzi, D., Németh, K., Geyer, A., Álvarez-Valero, A.M., Aguirre-Díaz, G., Bartolini, S., 2018. Historic hydrovolcanism at Deception Island (Antarctica): implications for eruption hazards. Bull. Volcanol. 80 (1), 1–28. https://doi.org/10.1007/s00445-017-1186-9.
Pedrazzi, D., Cerda, D., Geyer, A., Martí, J., Aulinas, M., Planagumà, L., 2022. Stratigraphy and eruptive history of the complex Puig de La Banya del Boc monogenetic volcano, Garrotxa Volcanic Field. J. Volcanol. Geotherm. Res. 107460 https://doi.org/10.1016/j.jvolgeores.2021.107460.
Pimentel, A., Pacheco, J.M., Felpeto, A., 2006. Influence of wind patterns on the dispersal of volcanic plumes in the Azores region: test study of the 1630 eruption of Furnas volcano (S. Miguel, Azores). Geophysical Research. Abstracts 8 (EGU06–A–04983).
Pimentel, A., Pacheco, J., Self, S., 2015. The ~1000-years BP explosive eruption of Caldeira Volcano (Faial, Azores): the first stage of incremental caldera formation. Bull. Volcanol. 77 (5), 1–26. https://doi.org/10.1007/s00445-015-0930-2.
Pimentel, A., Zanon, V., De Groot, L.V., Hipólito, A., Di Chiara, A., Self, S., 2016. Stress-induced comenditic trachyte effusion triggered by trachybasalt intrusion: multidisciplinary study of the AD 1761 eruption at Terceira Island (Azores). Bull. Volcanol. 78 (3), 1–21. https://doi.org/10.1007/s00445-016-1015-6.
Pimentel, A., Self, S., Pacheco, J.M., Jeffery, A.J., Gertisser, R., 2021. Eruption style, emplacement dynamics and geometry of peralkaline ignimbrites: insights from the Lajes-Angra Ignimbrite Formation, Terceira Island, Azores. Frontiers in Earth Sciences 9, 673686. https://doi.org/10.3389/feart.2021.673686.
Pioli, L., Erlund, E., Johnson, E., Cashman, K., Wallace, P., Rosi, M., Granados, H.D., 2008. Explosive dynamics of violent Strombolian eruptions: the eruption of Parícutin Volcano 1943–1952 (Mexico). Earth Planet. Sci. Lett. 271 (1–4), 359–368. https://doi.org/10.1016/j.epsl.2008.04.026.
Pyle, D.M., 1989. The thickness, volume and grainsize of tephra fall deposits. Bull. Volcanol. 51 (1), 1–15. https://doi.org/10.1007/BF01086757.
Pyle, D.M., 2000. Sizes of volcanic eruptions. In: Sigurdsson, H., Houghton, B.F., McNutt, S.R., Rymer, H., Stix, J. (Eds.), Encyclopedia of Volcanoes. Academic Press, San Diego, pp. 263–269.
Richter, N., Russell, J.M., Amaral-Zettler, L., DeGroff, W., Raposeiro, P.M., Gonçalves, V., Boer, E.J., Pla-Rabes, S., Hernández, A., Benavente, M., Ritter, C., Sáez, A., Bao, R., Trigo, R.M., Prego, R., Giralt, S., 2022. Long-term hydroclimate variability in the sub-tropical North Atlantic and anthropogenic impacts on lake ecosystems: a case study from Flores Island, the Azores. Quat. Sci. Rev. 285, 107525 https://doi.org/10.1016/j.quascirev.2022.107525.
Ritter, C., Gonçalves, V., Pla-Rabes, S., de Boer, E.J., Bao, R., Saez, A., Hernandez, A., Sixto, M., Richter, N., Benavente, M., Prego, R., Giralt, S., Raposeiro, P.M., 2022. The vanishing and the establishment of a new ecosystem on an oceanic island – Anthropogenic impacts with no return ticket. Sci. Total Environ. 830, 154828 https://doi.org/10.1016/j.scitotenv.2022.154828.
Saucedo, R., Macías, J.L., Ocampo-Díaz, Y.Z.E., Gómez-Villa, W., Rivera-Olguín, E., Castro-Govea, R., Sánchez-Núñez, J.M., Layer, P.W., Torres-Hernández, J.R., Carrasco-Núñez, G., 2017. Mixed magmatic–phreatomagmatic explosions during the formation of the Joya Honda maar, San Luis Potosí, Mexico. Geol. Soc. Lond., Spec. Publ. 446 (1), 255–279. https://doi.org/10.1144/SP446.11.
Secretaria Regional do Ambiente e do Mar, 2012. Plano de Gestão da Região Hidrográfica dos Açores RH9 - Caracterização da situação de referência e diagnóstico, vol. 8. Açores.
Smith, I.E.M., Németh, K., 2017. Source to surface model of monogenetic volcanism: a critical review. Geol. Soc. Lond., Spec. Publ. 446 (1), 1–28. https://doi.org/10.1144/SP446.14.
Smith, I.E.M., Blake, S., Wilson, C.J.N., Houghton, B.F., 2008. Deep-seated fractionation during the rise of a small-volume basalt magma batch: Crater Hill, Auckland, New Zealand. Contrib. Mineral. Petrol. 155 (4), 511–527. https://doi.org/10.1007/s00410-007-0255-z.
Stuiver, M., Reimer, P.J., Reimer, R.W., 2021. CALIB 8.2. [WWW program] at. http://calib.org. (Accessed January 2021).
Sulpizio, R., Mele, D., Dellino, P., Volpe, L.L., 2005. A complex, Subplinian-type eruption from low-viscosity, phonolitic to tephri-phonolitic magma: the AD 472 (Pollena) eruption of Somma-Vesuvius, Italy. Bulletin of Volcanology 67 (8), 743–767. https://doi.org/10.1007/s00445-005-0414-x.
Trippanera, D., Porreca, M., Ruch, J., Pimentel, A., Acocella, V., Pacheco, J., Salvatore, M., 2014. Relationships between tectonics and magmatism in a transtensive/transform setting: an example from Faial Island (Azores, Portugal). GSA Bull. 126, 164–181. https://doi.org/10.1130/B30758.1.
Vespermann, D., Schmincke, H.U., 2000. Scoria cones and tuff rings. In: Sigurdsson, H., Houghton, B.F., McNutt, S.R., Rymer, H., Stix, J. (Eds.), Encyclopedia of Volcanoes. Academic Press, San Diego, pp. 683–694.
Wilson, L., Walker, G.P.L., 1987. Explosive volcanic eruptions-VI. Ejecta dispersal in plinian eruptions: the control of eruption conditions and atmospheric properties. Geophys. J. Int. 89 (2), 657–679. https://doi.org/10.1111/j.1365-246X.1987.tb05186.x.
Wong, L.J., Larsen, J.F., 2010. The Middle Scoria sequence: a Holocene violent strombolian, subplinian and phreatomagmatic eruption of Okmok volcano, Alaska. Bulletin of Volcanology 72 (1), 17–31. https://doi.org/10.1007/s00445-009-0301-y.

Wood, C.A., 1980. Morphometric evolution of cinder cones. J. Volcanol. Geotherm. Res. 7 (3–4), 387–413. https://doi.org/10.1016/0377-0273(80)90040-2.

Zanon, V., Viveiros, F., 2019. A multi-methodological re-evaluation of the volcanic events during the 1580 CE and 1808 eruptions at São Jorge Island (Azores Archipelago, Portugal). J. Volcanol. Geotherm. Res. 373, 51–67. https://doi.org/10.1016/j.jvolgeores.2019.01.028.

Zanon, V., Pacheco, J., Pimentel, A., 2009. Growth and evolution of an emergent tuff cone: Considerations from structural geology, geomorphology and facies analysis of São Roque volcano, São Miguel (Azores). J. Volcanol. Geotherm. Res. 180 (2–4), 277–291. https://doi.org/10.1016/j.jvolgeores.2008.09.018.

Zawacki, E.E., Clarke, A.B., Arrowsmith, J.R., Bonadonna, C., Lynch, D.J., 2019. Tecolote volcano, Pinacate volcanic field (Sonora, Mexico): a case of highly explosive basaltic volcanism and shifting eruptive styles. J. Volcanol. Geotherm. Res. 379, 23–44. https://doi.org/10.1016/j.jvolgeores.2019.04.011.